Predicted ground motions for great interface earthquakes in the Cascadia subduction zone

Gail M. Atkinson and Miguel Macias

Abstract

Ground motions for earthquakes of **M**7.5 to 9.0 on the Cascadia subduction interface are simulated based on a stochastic finite-fault model, and used to estimate average response spectra for firm site conditions near the cities of Vancouver, Victoria and Seattle. The simulations are first validated by modeling the wealth of ground-motion data from the **M**8.1 Tokachi-Oki earthquake sequence of Japan. Adjustments to the calibrated model are then made to consider average source, attenuation and site parameters for the Cascadia region. This includes an evaluation of the likely variability in stress drop for large interface earthquakes, based on evaluation of data from other regions of the world in comparison to the Tokachi-Oki model predictions, and an assessment of regional attenuation and site effects.

We perform "best estimate" simulations for a preferred set of input parameters. Typical results suggest mean values of 5%-damped pseudo-acceleration in the range from about 100 to 200 cm/s^2, at frequencies from 1 to 4 Hz, for firm-ground conditions in Vancouver, Victoria and Seattle. Uncertainty in stress drop causes uncertainty in simulated response spectra of about ±50%. Uncertainties in the attenuation model produce even larger uncertainties in response spectral amplitudes – a factor of about two at 100 km, becoming even larger at greater distances. It is thus important to establish the regional attenuation model for ground-motion simulations. Furthermore, combining data from regions with different attenuation characteristics – in particular Japan and Mexico – into a global "subduction zone database" for development of global empirical ground-motion prediction equations, may not be a sound practice.

Time histories of acceleration for the stochastically-simulated motions are provided for reference sites in Vancouver, Victoria and Seattle. An alternative set of

motions, based on lightly modifying real recordings from the Tokachi-Oki to match expected conditions for Cascadia cities, are also provided. These alternative records have similar spectral content to the simulated motions, but contain additional complexity and more realistic phasing. The provision of alternative record sets allows users to conduct studies to determine the importance of these effects for structural response.

Introduction

This study uses a stochastic finite-fault model (Motazedian and Atkinson, 2005) to simulate time series and response spectra for scenario interface earthquakes of $\mathbf{M}$7.5 to 9.0 in the Cascadia subduction zone. An important feature of the approach is that the model is first validated using data from more than 300 strong-motion stations, at distances from 40 to 500km, for the September 26, 2003, $\mathbf{M}$ 8.1 Tokachi-Oki earthquake mainshock of Japan, and four of its aftershocks with $\mathbf{M}$ 7.3, 6.4, 5.9, and 5.5. We then modify the calibrated simulation model to consider appropriate source, attenuation and site characteristics for the Cascadia region. The simulations are produced for a firm reference ground condition in Victoria and Seattle (NEHRP B/C boundary) and Vancouver (top of the Pleistocene layer, with $Vs_{30} = 440$ m/s). A selection of the simulations is provided as an electronic supplement for the use of readers.

In a previous study (Macias et al., 2008), we used empirical regression analysis of the Japanese KNET Fourier spectral data to determine source, path and site characteristics of the Tokachi-Oki mainshock and its aftershocks. The ground motion attenuation for all the events can be modeled using an assumed geometric spreading coefficient $b_1 = -1.0$ with associated anelastic attenuation model given by an apparent $Q = 135 f^{0.76}$. By using dummy variables in the regression, site amplifications relative to NEHRP C sites were determined for D and E sites. Non linear site amplification was investigated for the $\mathbf{M}$ 8.1 data but was not significant in determining the overall amplification factors. Fourier spectra data were corrected to a reference near-source distance and site condition (hard rock). The source spectrum for each event was compared to that of a Brune-model spectrum, in order to compute seismic moment and stress drop. Stress drops range from 100 to 200 bars with no apparent dependence on

magnitude. The main shock stress drop was 120 bars. A similar value (100 bars) was calculated for an interface aftershock. Events with the highest stress drops (near 200 bars) may have been in-slab events.

In this study, we build on that work, using it to aid in predictions of motions from future great earthquakes (**M**>8) on the Cascadia subduction zone. We first confirm that a stochastic finite-fault model (Motazedian and Atkinson, 2005), based on the source and attenuation parameters determined for the Tokachi-Oki events (from the Fourier spectra), provides an excellent fit to the response spectral amplitude data for the event. Thus the Tokachi-Oki event provides a calibration event for the stochastic finite-fault technique, to demonstrate its applicability for the prediction of response spectra for great interface events. Then, we examine what modifications to the calibrated Tokachi-Oki model (source, path, site) are needed to apply it to the Cascadia setting. This includes an evaluation of the likely variability in stress drop for large interface earthquakes, based on evaluation of data from other regions of the world in comparison to the Tokachi-Oki model predictions. Finally, we simulate ground motions for earthquakes of **M**7.5 to 9 for selected Cascadia locations. These scenarios are mainly constrained by the observed average stress drop ($\Delta\sigma$) for interface earthquakes, by the limits for the possible rupture area of future large interface earthquakes in the region (Hyndman and Wang, 1995; Flück et al, 1997), and by regional attenuation. The simulations provide time histories and estimates of response spectra at selected cities, and we also express the response spectra as ground-motion prediction equations (GMPEs) for Cascadia events.

A significant feature of the study is that we provide not just response spectral estimates, but also time histories of acceleration. Time histories are needed as input to a variety of engineering and soil response methods. We recognize that stochastic methods are a simplistic way to simulate time histories, and may be missing potentially important coherent pulses and phasing information found in real records. This information could be particularly important for events with rich long-period energy, such as mega-thrust earthquakes. To address this, and facilitate studies that can assess the importance of these effects, an alternative set of time histories is developed, based on lightly modified real recordings of the Tokachi-Oki mainshock at appropriate distances, such that they carry

similar spectral content to that expected in Cascadia. (The elastic response spectra and durations of the modified-real and stochastically-simulated time histories are approximately equal, for the same magnitude and distance.) By comparing the response of structural systems or soils to the simulated versus the modified real recordings, we hope that future studies will provide insight into the important question of what record characteristics are most important.

We focus on three cities for this exercise: Vancouver, B.C. (Fraser Delta), Victoria, B.C. and Seattle, Washington. The simulated records, as well as the modified real records, are available as an electronic supplement (and by download from www.seismotoolbox.ca). The simulated records are intended to capture the gross characteristics of expected motions from Cascadia events in terms of amplitudes, frequency content and duration. The modified real records have similar underlying spectral content, but contain additional information on phasing and other features not embedded in the stochastic model. In neither case do we attempt to model specific wave propagation features, as these may be better addressed with detailed site-specific studies for given rupture scenarios, locations and site conditions.

Stochastic finite fault modeling of the M 8.1 Tokachi-oki earthquake

In this study we use the stochastic finite fault modeling approach of Motazedian and Atkinson (2005), as implemented in the computer code EXSIM, for the analysis and simulation of spectral ordinates of the September 26, 2003, **M** 8.1 Tokachi-Oki earthquake and some of its aftershocks. The method models ground motions as a propagating array of Brune point sources, each of which can be simulated using the stochastic point source methodology of Boore (1983, 2003). The low-frequency content is controlled by the seismic moment, while the high-frequency content is controlled by the stress drop of the subsources. The description of the modeling parameters is given after a brief summary of the data utilized to calibrate the model parameters.

Data

Three component acceleration records from the KNET seismic network (Kinoshita, S., 1998), for the **M** 8.1 Tokachi-oki earthquake and for some of its aftershocks (**M**: 7.3, 6.4, 5.9, 5.5), were downloaded from www.knet.bonsai.go.jp. The data range in distance from 40 to 500 km. Shear wave velocity and density data profiles, described down to 20 m in most of the cases, were also available for each station. A shear wave window, defined from the S-wave arrival up to a cut-off time equivalent to 90% of the signal energy, and baseline corrected, was applied to each record. Pseudo spectral accelerations for 5% damping (PSA) were calculated for all corrected records; we used the geometric mean of the two horizontal components, for frequencies from 0.1 to 10 Hz, as the ground-motion variable for modeling. We used the site classification reported by Macias et al. (2008) for the K-NET sites considered in this analysis. These authors followed the NEHRP scheme (BSSC, 2001), using procedures reported in Boore (2004) to extrapolate the velocity profiles from 10 or 20 m down to 30 m in order to obtain the appropriate average velocity over 30 m. Figure 1 shows the station locations, epicentres of main shock and selected aftershocks, a graphical representation of the main shock fault plane modified from Yagi (2004) and also summarizes site classification results.

Parameters of the stochastic finite-fault model

The parameters required for the stochastic finite fault method describe the source, path and site contributions to the simulated ground motions; in this case we calibrate these parameters using data from the **M** 8.1 Tokachi-Oki mainshock. For the selected aftershocks, we make minor modifications to the source parameters (ie. the stress drop) of each event, while holding site and path parameters constant for all events. The analysis for the selected aftershocks adds robustness to the model, providing insight into event-to-event variability in source and path effects.

Source: We follow Yagi (2004) to define most of the source parameters for the main shock, i.e.: fault geometry (length, wide, strike and dip angles of the fault plane) and slip distribution. For the aftershocks, the geometry is not known. Therefore, we used the Harvard moment tensor catalogue (HRV) at www.neictest.cr.usgs.gov/neis/sopar to

define seismic moment for each aftershock, and based its dimensions on the empirical relationships of Wells and Coppersmith (1994). Table 1 contains the source parameter values used in the simulations, along with the adopted path and site parameters (described next).

Path: The attenuation parameters for the simulations were adopted from Macias et al. (2008). Their reported attenuation model (geometric spreading and an-elastic attenuation parameters) is based on regression analysis of Fourier acceleration spectra (*Faccn*) of the same database analyzed here, from 0.1 to 10 Hz, for recordings at distances from 40 to 350 km from the fault plane (R_{cd}). The duration of ground motion as a function of distance is represented as: $T = T_0 + d \cdot (R)$. The source duration, T_0, depends on fault dimension and therefore magnitude. The distance-dependent duration slope (*d*) was determined by Macias et al. to have a value of 0.09 for the main shock; this is the fitted slope from plots of shear wave duration (up to 90 % of the signal energy) versus distance. It may be a slight overestimate of the distance-dependent duration effect from the point of view of simulations, as it is based on a long estimate of duration, out to 90% of signal energy. For the mainshock this effect is not particularly important, as the source duration dominates the signal duration. For the aftershocks we assigned a slightly smaller value of $d = 0.07$, as being more typical for most events (Atkinson, 1995; Beresnev and Atkinson, 1997).

Site: The site amplification functions for each site class (i.e. NEHRP C, D and E sites) were adopted from Macias et al. (2008). Macias et al. calculated the expected amplification for NEHRP C sites (their reference site condition) using the quarter wave length approach (Joyner et al, 1981; Boore and Joyner, 1997), for a shear wave velocity model that combined a typical C-site profile with a crustal model of the region (Iwasaki et al., 1989). To perform the calculations, they used the SITE_AMP computer code of Boore (2003), with an assumed angle of incidence $i = 45.0°$ and a kappa factor (Anderson and Hough, 1984) $\kappa = 0.045$. Their choice of $i = 45.0°$ was intended to reflect the shallow depth of the main shock and the large area coverage of data; their $\kappa = 0.045$ was the

observed κ_0 value based on fitting κ measurements from Fourier acceleration spectra data versus distance, mainly from the **M** 8.1 event.

The NEHRP C amplification function reported by Macias et al. is shown in Figure 2, and applied in our simulations for the Tokachi-Oki event. We also show the effect of changing i from 45.0° to 0.0° (vertical incidence) and κ from 0.045 to 0.02 in the NEHRP C amplification function. This illustrates that the reference amplification function is actually quite sensitive to these choices, especially at high frequencies. This is a factor that should be kept in mind in interpreting source parameters; for example, the stress drop will trade off against the reference amplification, with a higher site amplification implying a lower stress drop.

Stochastic Finite-Fault Results for Tokachi-Oki

We model the Tokachi-Oki mainshock and its aftershocks using the attenuation and site parameters defined above. For each event, we adjust the stress drop parameter to obtain the best match of simulations to data. This match is defined in terms of residuals, defined as the difference between the logarithmic values (base 10) of the observed and the simulated PSA ordinates:

$$res\ (f, R_{cd}) = \log_{10}(\text{PSA}_{obs})\text{-}\log_{10}(\text{PSA}_{sim}) \tag{1}$$

The best value of stress drop ($\Delta\sigma$) is that which minimizes the average residual, **stat1**, defined by:

$$\textbf{stat1} = \tfrac{1}{M}\sum_{n=1}^{N}\sum_{m=1}^{M}\left|res_{nm}(f, R_{cd})\right| \tag{2}$$

while the variability of the residuals is expressed by its standard deviation, **stat2**:

$$\textbf{stat2} = \left(\tfrac{1}{N}\sum_{n=1}^{N}\text{var}_n[res_n(f, R_{cd})]\right)^{1/2} \tag{3}$$

where N = number of frequencies, M = number of distances and var_n is the variance calculated on a residual vector distributed in distance for the nth frequency. The residuals were calculated at the NEHRP C reference level. The observed PSA ordinates on D and

E sites were first corrected to this reference level using the amplification functions of Macias et al. (2008) for D and E sites relative to C. Then, the corrected data were compared to the model defined for NEHRP C to calculate residuals.

We determined for each event the $\Delta\sigma$ value which minimizes the average residual, **stat1**. Figure 3 shows how the average residuals are distributed in frequency for the **M** 8.1 mainshock. To illustrate the effect of the amplification factor on the inferred solution, we present two cases: i) in which the reference NEHRP C amplification function is based on $\kappa = 0.045$ and $i = 45.0°$; and ii) in which the reference C amplification is based on the values calculated with $\kappa = 0.02$ and $i = 0.0°$. The inferred stress drop changes only slightly based on the assumed NEHRP C amplification (120 bars vs. 110 bars), but we note that the latter amplification function provides a better distribution of residuals across frequency, by accounting for apparent high-frequency energy in the PSA data. The strong signal at high frequencies is consistent with overall site conditions in Japan, which typically feature a shallow soil layer over rock.

Figure 4 plots residuals against distance, for two selected frequencies, for the interface events (**M** 8.1 and the **M** 6.4 aftershock) and for two aftershocks (**M** 7.3, **M** 5.9) believed to be in-slab events (Ito et al, 2004). There are no apparent trends of residuals with distance, indicating a good fit of the attenuation model to the data. Interestingly, the best-fit value of $\Delta\sigma$ appears to be about 100 bars for the interface events, compared to values near 200 bars for the suspected in-slab events. These stress drop values are in good agreement with the results reported by Macias et al. (2008) for these events based on near-source Fourier spectra, as would be expected. For the **M** 8.1 mainshock, the inferred stress drop agrees with the value of 120 bars reported by Yagi (2004).

Estimation of stress drop variability for large interface earthquakes

We have shown in the previous section that the stochastic finite fault modeling technique accurately reproduces, on average, observed ground motion characteristics (amplitudes and frequency content) from large interface earthquakes, once the regional source, path and site characteristics are known. The attenuation and site models can be

established regionally, at least in theory, from data of smaller magnitudes. However, we may be lacking sufficient information on source parameters. For example, for the Cascadia region we have empirical information on attenuation and site effects (Atkinson, 2005), but there is no information on the stress drop that might be expected for a great interface event. To place some constraints on this key uncertainty, we look at stress drop variability amongst large events on subduction interfaces worldwide.

Our approach is to perform simple comparisons between observed and simulated PSA values for selected interface earthquakes. We focus on model vs. data comparisons of spectral amplitudes at distances of about 60 ($\pm$ 20) km; in this distance range the observed motions are reduced by the geometric spreading attenuation factor (Crouse et al, 1988), but the anelastic attenuation factor (which may vary regionally) has a minor effect. The base simulation model for the comparisons is the Tokachi-Oki model as defined above. Predictions for this model are compared to PSA data from selected interface earthquakes of different subduction zones that have multiple recordings within 100 km of the fault (as compiled by Atkinson and Boore, 2003). Table 2 lists the selected earthquakes, along with moment magnitude, hypocentral and focal mechanism information from the Harvard Central Moment Tensor catalogue.

For the distance range of R_{cd} < 100 km, in which our comparisons are focused, we assume that the geometric spreading coefficient is b = -1.0 for all subduction regions, and that regional differences in anelastic attenuation behaviour are unimportant (Crouse et al, 1988; Youngs et al, 1997; Atkinson, 2005). We make a preliminary estimation of likely regional crustal amplification effects that would apply (as described below). By comparing simulated amplitudes from the Tokachi-Oki model (adjusted for regional crustal amplification) with various $\Delta\sigma$ values to observed amplitudes, we make an estimate of the $\Delta\sigma$ value for each the selected earthquakes. It is acknowledged that these are rough estimates, as we make no attempt to model attenuation and site processes in detail for each event. The aim is simply to gain insight on the likely variability of $\Delta\sigma$ for large interface events.

The reference site condition for the comparisons is the NEHRP B/C boundary (V_{S30} = 760 m/s). The AB03 database provides site classification (from NEHRP A to NEHRP

E classes) for each record. We assigned fixed representative values for each class: $V_A =$ 2000 m/s; $V_B =$ 1050 m/s; $V_C =$ 560 m/s; $V_D =$ 270 m/s; $V_E =$ 100 m/s. The amplification factors by which to correct each record to the corresponding PSA values for B/C site conditions were obtained by using the empirical site amplification relationships given by Boore and Atkinson (2007); for consistency and simplicity, the expected peak ground acceleration for B/C conditions ($PGA_{B/C}$) to input to these relationships was calculated using their prediction equation for $PGA_{B/C}$. The value for $PGA_{B/C}$ is only a preliminary estimate; the amplification factors are not particularly sensitive to this value. To produce simulations for B/C boundary conditions for Tokachi-Oki, we used the site information provided by K-NET, selecting stations that lie between B and C (stations IWT from 008 to 010 and MYG from 001 to 004) to define a generic shear-wave velocity and density profile for B/C conditions. We calculated the amplification function for this profile using Boore's (2003) SITE AMP program. We assumed vertical incidence and $\kappa = 0.02$ for the calculations (as kappa is expected to be lower for B/C sites than for softer site conditions). Further details are provided in Macias (2008) and Atkinson and Macias (2008).

The amplification function for B/C sites may be expected to show significant regional variability due to typical crustal conditions, especially at high frequencies (Crouse et al, 1988; Atkinson and Boore, 2003; Atkinson and Casey, 2003). Consequently, in our comparisons the observed spectral ordinates at high frequencies may be influenced by both the stress drop of the event and the regional crustal amplification. To account for this effect, we calculated an expected B/C amplification function for each region. We compile, from different sources of information, shear velocity and density crustal models (Alaska: Niazi and Chun, 1989; Brocher et al., 2004. Chile: Mendoza et al., 1994. Japan: Iwasaki et al., 1989; Nishizawa and Suyehiro, 1986. Mexico: Valdes et al., 1986; Furumura and Singh, 2002; Dominguez et al., 2006), and define an average model for each region. These models define the conditions of the crust in each region, but typical conditions in the upper 30 m are not known. We therefore adopt the top 30 m B/C shear velocity profile defined for Japan as a generic top 30 m B/C profile for all regions. Figure 5 shows the B/C amplification functions for each region under this assumption, calculated for $\kappa = 0.02$ and $i = 0.0°$. (Note: more details on the

velocity profiles and amplification functions are provided in Macias, 2008). Figure 5 suggests remarkable differences in expected amplifications at frequencies below 1 Hz between regions. However at high frequencies the amplifications are similar, which is not surprising given the common site profile for the top 30 m. This commonality of behaviour at high frequencies means that the calculated stress drops will be insensitive to the regional amplification function, as it is the high frequencies that control stress drop. This is an aspect of the study that could be improved in the future if more information on typical site conditions and their effect on high frequency amplitudes become available.

In Figures 6 to 8, we show (for B/C boundary site conditions) the simulated versus observed PSA at 10 Hz, for the selected earthquakes. Plots were also made for 5 Hz, but are not shown as they indicate the same results as those for 10 Hz. Based on inspection of these plots, we made a rough estimate of stress drop for each event, as listed in Table 3. The plots show some interesting differences and agreements in attenuation behaviour between the Tokachi model and data from various regions. We minimized the effect of these differences by focusing on the comparisons at distances < 100 km to draw conclusions regarding stress drop. No fitting of the data to the model calculations is performed, as we do not feel it is warranted given the lack of region-specific information on attenuation and site conditions. The stress drop estimates are a judgement based on inspection.

Based on these results, and considering that unaccounted-for site effects or erroneous information on site classification may be present in the data, we adopted as the lower limit of $\Delta\sigma$ for interface earthquakes a value of **30 bars.** This value is supported by the stable estimates of stress drop from the Alaska region that suggest this value, and by the lower limits for some of the Mexican earthquakes. For the upper limit on stress drop, we set a value of **150 bars.** The selection of this value was not as clear as the lower limit; there may be some higher values, such as the inferred values of up to 170 bars for the Chilean and Japanese earthquakes. On the other hand, there are some events for which a value of 120 bars appears relatively well defined (including the Tokachi-Oki mainshock). On balance, we selected 150 bars as an upper limit of $\Delta\sigma$ for interface earthquakes. This is not intended to be an absolute upper limit, nor is 30 bars intended to

be an absolute lower limit. Rather these represent what may be considered as values that are perhaps one to two standard deviations from a median value. A more precise representation of stress drop variability must await more detailed studies of this parameter for large interface events.

Ground motion predictions for the Cascadia subduction zone

We use the calibrated EXSIM model to simulate ground motion for generic sites in Southwestern British Columbia and Northwestern Washington. The simulation scenarios are constrained by the geometry of the anticipated rupture area (Hyndman and Wang, 1995; Flück et al, 1997), the average stress drop for subduction zone earthquakes and its variability (as estimated above), and by regional estimates of attenuation and site conditions. We begin by generating simulations for our "best estimates" of these parameters, then explore the implications of alternative values for the main uncertainties in source and attenuation parameters.

Source

For the seismic source geometries we follow Hyndman and Wang (1995), who define the landward limit of the rupture surface based on the geometry and temperature gradient of the slab. We generate response spectral ordinates (PSA) for the average stress value $\Delta\sigma$ = 90 bar, for moment magnitudes **M** 7.5, 8.0, 8.5, and 9.0, for three specific reference site locations and reference conditions. The locations, and their corresponding generic site conditions, are chosen to correspond to firm sites in: (i) the Fraser Delta region of Vancouver (FRA); (ii) Victoria (VIC); and (iii) Seattle (SEA). To simulate the motions at each location we locate the fault plane symmetrically about a perpendicular line from the trench to the site. Fault plane areas for each magnitude were defined considering the relationships used by Wells and Coppersmith (1994), Kanamori and Anderson (1975), and Beresnev and Atkinson (1997). Once an average area was defined, the fault length for the **M** 8.0 and **M** 8.5 cases was assigned a 90 km fixed fault width (this is the maximum according to Hyndman and Wang). The **M**7.5 event was assigned a narrower width, based on Wells and Coppersmith (1994). For the **M** 9.0 Cascadia

scenario (Satake et al, 1996), we considered both the 90 km width, and a wider rupture zone of 150 km, with the fault length adjusted accordingly. Figures 9 and 10 show the fault planes that correspond to the FRA, VIC and SEA simulations respectively, while Table 4 lists the simulation geometries and parameters. All simulations assume random slip distribution and random hypocenter location on the fault plane.

Path

Attenuation of ground motions in the Cascadia subduction zone was investigated by Atkinson (2005), using empirical data from earthquakes of small-to-moderate magnitude. Her findings suggest that the empirical attenuation model used for California by Atkinson and Silva (2000) (AS00) may be appropriate to express attenuation for offshore events in the area of the subduction zone. We adopted the AS00 attenuation model as our "best estimate" attenuation model. The distance-dependent duration of motion term is taken as 0.10 based on typical values shown by Raoof et al. (1999) (from which the AS00 model was derived); this factor is not important as source duration dominates the total duration.

Site

We calculated generic site amplification factors for reference "firm" sites as a function of frequency for Vancouver's Fraser delta, Victoria and Seattle (FRA, VIC and SEA). Amplifications are constructed separately for each location, as studies suggest there are significant differences in shallow crustal structure. For example, a thinner layer of accreted sediments lies beneath Victoria in comparison to that beneath the Fraser delta or Seattle (Ramachandran et al, 2006; Graindorge et al, 2003; Ellis et al, 1983; McMechan and Spence, 1983). In the Fraser delta, there is a pervasive layer of Pleistocene deposits that overlies the tertiary bedrock; the Pleistocene layer has a stable shear velocity gradient from 400 to 1000 m/s, while the tertiary bedrock has an average Vs = 1500 m/s (Hunter, 1995; Hunter et al., 1997). For the Fraser delta, we selected the top of the Pleistocene as the reference site condition (V_{S30}=414 m/s), while for Victoria

and Seattle we define a generic NEHRP B/C boundary profile for the top 30 m (V_{S30}=760 m/s); this is firmer (and faster) than the conditions at the top of the Pleistocene layer that underlies the Fraser delta.   For each generic profile, the quarter wave length approach with an angle of incidence $i = 0.0°$ was used to compute the amplifications, assuming $\kappa = 0.02$ for NEHRP B/C boundary site conditions (VIC and SEA) and $\kappa = 0.03$ for FRA conditions (Pleistocene). Figure 11 plots the shear wave velocity profiles versus depth, while Figure 12 shows the amplification functions (see Macias, 2008 for details).

Each of our reference site conditions is somewhat arbitrary, and does not necessarily represent a specific site in any of the three studied areas. The generic profiles are intended to reflect shallow crustal properties and average local site conditions for the firmest sites that may be available; these motions may in turn be input to overlying soil deposits where applicable. For example, in Seattle several studies demonstrate the presence of soft and thick sediment layers which form the sedimentary basin structure on which Seattle is located (Frankel et al., 1999 and 2002; Jones, 1999). However, stiffer site conditions are found to the West and Southeast of Seattle, for example, at Tertiary sandstones at Alki Point and Seward Park, or recent glacial tills at Central Seattle and the Space Needle (Williams, 1999). These firmer sites were used to define the generic NEHRP B/C boundary site profile for Seattle. For Victoria, it is also possible to find B/C site conditions; according to Finn et al. (2004), nearly 50 % of shallow soil sites in Victoria would be classed between NEHRP A and C. Finally, for Vancouver, even though most of the Fraser delta has been classified as NEHRP D or E, there exist NEHRP C sites with velocities close to our adopted Pleistocene reference value of $V_{S30} = 414$ m/s in the Surrey Uplands, and within the City of Vancouver to the East and North of the Fraser Delta (Hunter et al., 2002). Thus we believe that our adopted reference models represent realizable "firm" reference site conditions in each of the studied areas.

"Best Estimate" Simulation Results

Figure 13 shows the average 5% damped pseudo-acceleration (PSA) at Victoria (B/C), Seattle (B/C) and Vancouver (C), for **M**8, 8.5 and 9 (c); distances from the fault are approximately 85 km, 120 km and 145 km, respectively. Time histories of

acceleration for these "best estimate" simulations ($\Delta\sigma$ = 90 bars, AS00 attenuation), for **M**8.5 and **M**9 (c) are provided in the electronic supplement for10 simulations. By running the simulation model for 100 trials, we determined that the random variability in simulated PSA values is around 20 % to 30 % of the average PSA values over all frequencies. Note that this represents only variability in the random simulation parameters (hypocenter, slip distribution, random seed), and is not a full measure of aleatory variability in expected ground motions; similarly, epistemic uncertainty is not included in this variability band.

Effect of Parameter Uncertainties

One of the key uncertainties in the source parameters that control ground motion amplitudes is the subevent stress drop parameter. Our "best estimate" response spectra assumed a value of $\Delta\sigma$ = 90 bars. On Figure 14, we show the effect of stress drop values of 30 and 150 bars (these are our estimates of the lower and upper limits on stress drop parameter based on interface events around the world) for a **M**9 scenario (the effect is similar for other magnitudes). Figure 15 suggests that uncertainty in ground motion spectral amplitudes for Cascadia events due to uncertainty in the appropriate stress drop parameter is about ±50 %; this uncertainty is partly epistemic (we do not know the median stress drop value) and partly aleatory (the stress drop for individual events will vary about the median).

Another important uncertainty in source characterization is the source geometry. This is particularly critical for the **M** 9 scenario due to its large extent. We therefore considered three possible geometries (Figure 10), including an elongated (1000 km x 90 km) fault geometry at two different orientations (geometries a, b) and a broader (600 km x 150 km) fault geometry (c).   The two orientations are used for the long, skinny fault plane because EXSIM models the fault plane as a straight line in plan (future enhancements could improve this to allow the fault plane to be a curve in plan);   thus the approximation of a curved fault trend by a straight line is an area of modeling uncertainty. Figure 15 shows the effect of these choices on the average PSA for simulated **M**9 events; the PSA for **M**8.5 is also plotted for reference. It is interesting to

note that the elongated geometry implied by a narrow 90 km fault rupture width implies lesser ground motions than would a wider fault zone; this is because the longer rupture results in much of the ground motion being generated at larger distances from the site. In fact, if the **M**9 event is truly a very long narrow rupture, then the motions it produces at seaboard cities may be lower than would be produced by an event of **M**8.5, especially at high frequencies.

A key uncertainty in the path model is the regional attenuation model, which includes both the geometric and anelastic attenuation effects. For our best estimates we adopted the Atkinson and Silva (2000) (AS00) attenuation model, based on the results of Atkinson (2005) for Cascadia events. Figure 16 explores the influence of possible alternative models to AS00 *(Q = $180 f^{0.45}$ and b_1 = [-1.0; -0.5] for [$R \leq 40$; $R > 40$ km])*, including those of Ordaz and Singh (1992) for Mexico (OS92) *(Q = $273 f^{0.66}$ and b_1 =* [-1.0; -0.5] for [$R \leq 100$; $R > 100$ km]), and Macias et al. (2008) for Japan (TK07) *(Q =* $135 f^{0.76}$ and b_1 = -1.0 for $R \geq 40$ km) for a site at typical distance (Seattle). In these comparisons the source and site parameters are fixed at the best estimate values. On Figure 16 we also plot the PSA estimates obtained from the empirical ground motion relationships for subduction zones reported by Atkinson and Boore (2003; 2008) (AB03), for the Cascadia region. It is interesting to note that the TK07 model represents a steeper attenuation compared to the other models; this is likely due to the strong attenuation observed on back arc sites of the Hokkaido region (Macias et al., 2008). By comparison, the rest of the models basically reflect fore arc attenuation conditions. There are significant differences in the attenuation effects (factor of 1.5-2.0) between the AS00 and OS92 models at low and high frequencies (though their predictions are similar at intermediate frequencies); this likely reflects actual attenuation differences between the central Mexico subduction zone and the Cascadia (SW Canada-NW United States) subduction zone. The AB03 results are a "compilation" from all zones, but may be biased by the predominance of records from Mexico for the large interface events. The underlying generic site effects for the AB03 database are unknown, but appear to be different from those inferred for Cascadia, based on differences in spectral shape; it is also possible that a spectral shape error in AB03 (Atkinson and Boore, 2008) is influencing the Cascadia shape, even though this error does not directly affect

computations when using the Cascadia regional factors. These results points to the importance of regional variations in attenuation and site effects in controlling ground motion amplitudes and spectral shapes, and suggest that the use of empirical subduction relations based on a mixture of data from around the world, though a traditional expediency, may not be a well-founded approach.

Attenuation of Interface Motions with Distance

The evaluation of parameter uncertainties above points to the potential importance of regional attenuation in controlling the expected amplitudes from Cascadia interface events. Figure 17 shows the expected decay of amplitudes (0.5 Hz and 5 Hz) with distance from the trench, for profiles that run perpendicular to the trench in southwestern B.C., as shown in Figure 18 with black square symbols (assuming the VIC B/C site conditions). All calculations use the "best estimate" AS00 attenuation model with $\Delta\sigma =$ 90 bars; results from 30 simulations were averaged to establish the mean PSA. The effect of magnitude is clearly much more important at lower frequencies, which is to be expected. On Figure 19, we show the importance of the attenuation model used by plotting the attenuation along the profile for a single magnitude, but for different attenuation models (average of 10 simulations); the empirical attenuation predictions of Atkinson and Boore (2003) (Cascadia factors) are also shown for comparison. The flat attenuation characteristics of the AB03 estimates relative to what is expected for Japan, and for Cascadia at lower frequencies, is apparent on this figure. The flat AB03 attenuation shape is likely a consequence of the fact that they are data-driven empirical relationships, derived from a database for which approximately 40% of the interface earthquakes occurred in the Mexican subduction zone. Studies have shown that earthquakes in the Mexican subduction zone exhibit a very slow ground motion attenuation with distance; the suggested cause is a regional amplification effect that is predominant for low frequencies at large distances (200 km and above) (Cardenas and Chavez-Garcia, 2003). The Mexican attenuation model shown in Figure 20 (Ordaz and Singh, 1992) is steeper than the Cascadia/California attenuation model (Atkinson and Silva, 2000) from 50 to 100 km (as the transition from body-wave to surface-wave

spreading rates occurs at greater distance in OS92 compared to AS00), but less steep at greater distances, for which the effects of higher Q in Mexico become more important. Nevertheless, it is encouraging (and perhaps fortuitous) that the AB03 relations agree quite well with the expected average PSA values for Cascadia at distances near 100 km, where the major cities are located.

Ground motion prediction equations for NEHRP B/C site conditions

The response spectral values from the simulation results for various magnitudes and distances (Figure 17) can be generalized for ease of use by fitting them to a ground-motion prediction equation (GMPE). We first verified that the results of Figure 17 are robust with respect to variations in site locations, by considering a "fan" of sites as shown in Figure 18, rather than just a single profile. The fan array covers 180° in 30° increments from the strike direction at distances of 30, 60, 100, 150, 200 and 400 km from the centre of each fault plane. (We also tested robustness to results by testing alternative subsource sizes and numbers of simulation iterations.) Figure 20 shows the simulation data generated for the fan of sites, in comparison to the GMPEs we developed to describe them.

A two-step linear regression procedure was applied to the simulated PSA ordinates for all magnitudes, to generate GMPEs for large interface earthquakes in the Cascadia region, for B/C site conditions. In the first step we determine the distance attenuation term plus a source term for each scenario (**M** 7.5, 8.0, 8.5, 9.0 (geometry c)) according to the form:

$$\text{Log } Y = \sum C_i\, E_i - C_1 \log R - C_2\, R \qquad\qquad (4)$$

where Y is the PSA value at a selected frequency, E_i is a dummy variable that has the value 1 for earthquake i and 0 otherwise, and $R = \sqrt{(R_{cd}^2 + h^2)}$. R_{cd} is the closest distance to fault, and h represents a near-source saturation term determined to provide the best fit to the shape for locations close to the fault plane. The second regression step determines the magnitude-dependent coefficients from the source terms C_i to:

$$C_i = C_0 + C_3 \, (\textbf{M}\text{-}8) + C_4 \, (\textbf{M}\text{-}8)^2 \qquad\qquad (5)$$

Residuals between the simulated and estimated log PSA (from Equation 4) were assessed, for different h values and for each scenario magnitude, to explore the dependency of h on magnitude. Based on modeling the shape of the PSA attenuation curves near the fault plane we determined the best value h for each magnitude, which is well-described by the following equation:

$$h = \textbf{M}^2 - 3.1 \, \textbf{M} - 14.55 \qquad\qquad (6)$$

It can be seen in Figure 20 that the GMPEs match the simulation results well. Table 5 contains the regression coefficients (Equations 1 and 2), which are applicable for B/C boundary site conditions. It is noted that the standard deviation of the equations (variability of ground motions) is not available from our procedure, as it is based on limited simulations and modeling. For use in seismic hazard calculations, we recommend that an estimate of variability from data-based regression models be used. Similarly, for other site conditions we recommend application of the site factors given by other empirical studies. The results of Boore and Atkinson (2007) for shallow crustal earthquakes in active tectonic regions would be a reasonable basis for estimating both the variability and site effects.

Figure 21 compares our GMPEs for interface events on the Cascadia subduction zone, for **M** 8.0 and 9.0 for rock conditions, to the predictions of theYoungs et al. (1999) (YS99), Gregor et al (2002) (GR02), and Atkinson and Boore (2003; 2008) (AB03, Cascadia) model. There are significant differences in the shape of the models, particularly at very large magnitudes, with this study tending to indicate steeper attenuation. The steeper attenuation predicted for Cascadia is driven by attenuation observed in western North America, as compared to other models that are significantly influenced by attenuation observed in Mexican data (Youngs et al., 1997 and Atkinson and Boore, 2003). Perhaps fortuitously, the models are in reasonable agreement (within about a factor of 2) at distances near 100 km, at which most major coastal cities are located.

Modified Tokachi-Oki Time Histories to Represent Cascadia Earthquakes

To this point we have produced time series and response spectra for the reference site condition for Vancouver (on Pleistocene NEHRP C), Victoria (NERHP B/C) and Seattle (NEHRP B/C), based on stochastic finite-fault simulations. The simulated motions contain the salient information on the predicted amplitudes, frequency content and duration for great subduction earthquakes. However, stochastic simulations have significant limitations in that they assume stationarity and random phase. They may be missing important additional information on coherent pulses that could affect response, particularly nonlinear response to long-period structures. It is therefore useful to also consider "real" earthquake records for analysis. No strong-motion records exist for great earthquakes on the Cascadia subduction zone. However we may derive a proxy for such records, by making suitable modifications to actual time histories from the Tokachi-Oki mainshock.

The modification technique is a variation on the classic "spectrum matching" technique (McGuire et al., 2001; see also COSMOS, Technical Meeting 2005 http://www.cosmos-eq.org/TS2005.html) in which selected real earthquake records are modified in the frequency domain (or time domain) such that their response spectra will more closely match a specified target spectrum. Records are input to an algorithm that modifies them by enhancing amplitudes at some frequencies while suppressing amplitudes at others, such that the spectral content of the modified record matches the target spectrum. A key advantage of this technique is that the phase characteristics of the record are not modified, and thus it retains the character of the original earthquake time history, including any important pulses that the record may contain. This method is most typically used iteratively, bringing the records progressively closer to a smooth target spectrum, until the desired degree of match to the target is obtained. However there is a significant drawback to spectrum matching to a smooth target; it removes the peaks and troughs (variability with frequency) in the response of natural (unaltered) records. Recent studies (Luco and Bazzurro, 2007) suggest that the removal of these peaks and troughs through spectral matching could reduce the response of structures by as much as

30%. The reason is believed to be related to the asymmetric effect that peaks and valleys in the elastic spectrum of real records have on nonlinear structural response (Carballo and Cornell, 2000). In this sense, the spectral matching approach could be unconservative, rendering real records more benign.

To obtain the benefits of spectral matching without reducing natural peak-to-trough variability, we use a 'frequency-dependent scaling' approach wherein records are only lightly modified, and in such a way as to preserve variability with frequency. The inputs to the method comprise a smooth target spectrum plus a 3-component record selected in the appropriate magnitude-distance range and having suitable spectral shape (not too divergent from the target). We take the ratio of the observed response spectrum of the selected natural record to the target response spectrum, over the frequency range of interest for the time history (eg. 0.2 – 20 Hz). The trend of this ratio should be relatively smooth in frequency on average (if candidate records have suitable shape), but will have peaks and troughs from the natural record. A smooth polynomial is fit to the ratio in log-log space (thus we fit log Ratio versus log frequency). An example is shown in Figure 22. The polynomial is then used as a single-iteration spectral modification function in the spectral-matching approach. This is done by dividing the Fourier transform of the input earthquake record by the factor obtained from the polynomial function. (Note: for frequencies outside the range of the low- or high-frequency limits of the assessed polynomial, a constant value equal to that at the corresponding frequency limit is applied.) High-pass and low-pass filters are used to control the amplitudes of the Fourier spectrum beyond the frequency range fitted by the polynomial. The modified record is obtained by Fourier transform back to the time domain. Each record is checked to ensure that the modified acceleration, velocity and displacement traces are reasonable, and similar to the corresponding input records in character.

The polynomial function is essentially a frequency-dependent scaling factor, as opposed to a constant scaling factor. The frequency-dependent scaling approach generates a lightly-modified natural record that approximates the target UHS over a selected frequency range, but does not remove natural peaks and troughs. The record will not match the target spectrum as closely as traditional spectrally-matched records, but will meet it on average over the specified frequency range. We choose to have the two

horizontal components retain their relative amplitudes (in natural records, one horizontal component will be larger than the other), by using a single polynomial function based on the average of the two horizontal components (rather than scaling each horizontal component to the target individually). This same function can also be applied to the vertical component record (if there is not a specific vertical target).

To apply the frequency-dependent scaling approach to Cascadia, we selected three Tokachi-Oki input accelerogram in the appropriate distance range, recorded on NEHRP C sites. The selected stations are HKD 084 (at 72 km from the fault rupture), HKD 101 (at 117 km) and HKD 124 (at 148 km). Their spectra are shown in Figure 22; a linear scaling factor of 2.5 was applied to the vertical-component record of HKD 084, and a factor of 2.0 was applied to the vertical-component record of HKD 124, to bring the long-period levels of these components up to that of the horizontal components (the original vertical-component records at these stations are weak relative to the horizontal). These input records are "frequency-dependent scaled" to the target mean response spectra determined by the simulations (90 bars, AS00 attenuation) for Vancouver (on Pleistocene, NEHRP C), Victoria (on NEHRP B/C) and Seattle (B/C) (as shown in previous sections). We selected the target magnitude of $\mathbf{M}$8.5 (slightly larger than the Tokachi-Oki event). For each station, we took the log ratio of the recorded response spectrum (log average of the two horizontal components) to the target, over the frequency range from 0.2 – 20 Hz, and fit it with a polynomial in log Ratio versus log frequency; the polynomial ranges in order from 3 to 5 as required to provide a fit to the shape of the ratio data. We divided the Fourier transform of each baseline-corrected record by the frequency-dependent scaling factors defined by the polynomial, and applied a 4th order Butterworth filter at 0.1 Hz (low-cut) and 30 Hz (high-cut). The reverse Fourier transform produced the lightly-modified time histories. This procedure was applied to each of the horizontal components, plus the vertical component (same polynomial function). The modified three-component records are included in the electronic supplement.

Figure 23 provides an example comparison of the spectra of the modified records to the target for Victoria; additional plots are provided in Atkinson and Macias (2008). The spectra of the lightly-modified records match the target reasonably well, while

maintaining significant natural frequency-to-frequency variability. The average of the horizontal components for all 3 stations does a reasonable job of matching the target overall. The procedure will not necessarily provide a close match over all frequencies, and it is important to note that it is not intended to do so. The vertical-component records have spectra that match the horizontal target at low frequencies, while being lower in amplitude at high frequencies. This is in accordance with typical H/V ratios that suggest that the vertical component is about two/thirds of the horizontal at high frequencies for rock sites (Siddiqqi and Atkinson, 2002). Figure 24 shows an example of the original and modified time series, in acceleration, velocity and displacement, illustrating that the essential character of the records is not changed by the process. The electronic supplement provides the lightly-modified accelerograms, appropriate for a **M**8.5 Cascadia earthquake on firm ground conditions at Victoria, Vancouver and Seattle. The response of structural systems to these records can be compared to that for the corresponding stochastically-simulated records for **M**8.5 in order to gain insight into what record characteristics drive response.

Conclusions

Ground motions for earthquakes of **M**7.5 to 9.0 on the Cascadia subduction interface were simulated based on a stochastic finite-fault model, and used to estimate average response spectra for firm site conditions near the cities of Vancouver, Victoria and Seattle. An important attribute of the simulations is that they were first validated by reproducing the wealth of ground-motion data from the **M**8.1 Tokachi-Oki earthquake sequence of Japan. Adjustments to the calibrated model were then made to consider average source, attenuation and site parameters for the Cascadia region.

The simulations provide estimates of response spectra for firm-site conditions (B/C boundary in Victoria or Seattle, or top of the Pleistocene in Vancouver); these motions could be input at the base of a soil layer to consider other site conditions which may amplify the motions. To allow the reader to use the time series for such purposes, we provide a selected set of simulations (10 trials per location, for Vancouver, Victoria and Seattle, for **M**8., 8.5 and 9.0 c) as an electronic supplement.   The simulations are

provided for our "best estimate" parameters – a stress drop of 90 bars, with the Atkinson and Silva (2000) attenuation model. In recognition that "real" time histories may contain important information on phasing, and long-period pulses, that are not generated by stochastic simulations, we also provide time histories developed by a light spectral modification of Tokachi-Oki records at selected sites; these records provide more realistic time series, but mimic the spectra expected for the reference condition at each city. It is recommended that users consider both the simulated and modified real recordings, to determine whether response is affected by the characteristics of real recordings not included in generic stochastic simulations.

As well as performing "best estimate" simulations for a preferred set of input parameters, we considered the effects of uncertainty in source and attenuation. We conclude that uncertainty in stress drop causes uncertainty in simulated response spectra of about ±50%. Uncertainties in the attenuation model produce even larger uncertainties in response spectral amplitudes – a factor of about two at 100 km, becoming even larger at greater distances. This points to the importance of establishing the regional attenuation model for ground-motion simulations. It also suggests that combining data from regions with different attenuation characteristics – in particular Japan and Mexico – into a global "subduction zone database" for development of global empirical ground-motion prediction equations, may not be a sound practice.

Acknowlegements

References

Anderson, J., and S. Hough (1984). A model for the shape of the Fourier amplitude
spectrum of acceleration at high frequencies. Bull. Seism. Soc. Am., **74**, 1969-
1993.

Atkinson, G. (1995). Attenuation and source parameters of earthquakes in the Cascadia
region. Bull. Seism. Soc. Am., **85**, 1327-1342.

Atkinson, G. (1996). The high-frequency shape of the source spectrum for earthquakes in
eastern and western Canada. Bull. Seism. Soc. Am., **86**, 106-112.

Atkinson, G. (2005). Ground motions for earthquakes in South-western British Columbia
and North-western Washington: crustal, in-slab, and offshore events. Bull. Seism.
Soc. Am., **95**, 1027-1044.

Atkinson, G., and D. Boore (2003). Empirical ground-motion relations for subduction
zone earthquakes and their applications to Cascadia and other regions. Bull.
Seism. Soc. Am., **93**, 1703-1729.

Atkinson, G., and D. Boore (2008). Erratum: Empirical ground-motion relations for
subduction zone earthquakes and their applications to Cascadia and other regions.
Bull. Seism. Soc. Am., **98**, in press.

Atkinson, G., and R. Casey (2003). A comparison of ground motions from the 2001 M
6.1 in-slab earthquakes in Cascadia and Japan. Bull. Seism. Soc. Am., **93**, 1823-
1831.

Atkinson, G. and M. Macias (2008). Predicted ground motions for great Cascadia
interface earthquakes. Report to U.S. Geol. Surv. NEHRP Grant 07HRGR0041.
http://earthquake.usgs.gov/research/external/. Last accessed June 2008.

Atkinson, G., and W. Silva (1997). Empirical source spectra for California earthquakes.
Bull. Seism. Soc. Am., **87**, 97-113.

Beresnev, I., and G. Atkinson (1997). Modeling finite-fault radiation from the ω^2
spectrum. Bull. Seism. Soc. Am., **87**, 67-84.

Boore, D. (1983). Stochastic simulation of high-frequency ground motions based on seismological models of the radiated spectra. Bull. Seism. Soc. Am., **73**, 1865-1894.

Boore, D. (2003). SMSIM – Fortran programs for simulating ground motions from earthquakes: version 2.2, *U.S. Geol. Surv.* A modified version of OFR 00 – 509, 56 pp.

Boore, D. (2004). Estimating $\overline{V}_s(30)$ (or NEHRP site classes) from shallow velocity models (depths < 30 m). Bull. Seism. Soc. Am., **94**, 591-597.

Boore, D.M., and G. Atkinson (2007). Boore-Atkinson NGA Empirical Ground Motion Model for the Average Horizontal Component of PGA, PGV and SA at Spectral Periods of 0.1, 0.2, 1, 2, and 3 Seconds, www.peer.berkeley.edu, June 2006.

Boore, D.M., and W.B. Joyner (1997). Site amplifications for generic rock sites. Bull. Seism. Soc. Am., **87**, 327-341.

Brocher, T. M., G. S. Fuis, W. J. Lutter, N. I. Christensen, and N. A. Ratchkovski (2004) Seismic velocity models for the Denali fault zone along the Richardson highway, Alaska. Bull. Seism. Soc. Am., **94**, S85-S106.

Building Seismic Safety Council (BSSC) (2001). NEHRP recommended provisions for seismic regulations for new buildings and other structures, 2000 Edition, Part 1: Provisions, prepared by the Building Seismic Safety Council for the Federal Emergency Management Agency (Report FEMA 368), Washington, D.C.

Carballo, J. and A. Cornell (2000). Probabilistic seismic demand analysis: spectrum matching and design. Rpt. No. RMS-41; Dept. Civil and Env. Eng., Reliability of marine structures program, Stanford Univ., Palo Alto, CA.

Cárdenas-Soto, M. and F. J. Chávez-García (2003). Regional path effects on seismic wave propagation in central Mexico. Bull. Seism. Soc. Am., **93**, 973-985.

Crouse, C. B., K. V. Yogesh, and B. Schell (1988). Ground motion from subduction-zone earthquakes. Bull. Seism. Soc. Am., **78**, 1-25.

Domínguez, J., G. Suárez, D. Comte, and L. Quintanar (2006). Seismic velocity structure of the Guerrero gap, Mexico.Geofisica Internacional, **45**, 129-139.

Ellis, R. M., G. D. Spence, R. M. Clowes, D. A. Waldron, and I. F. Jones (1983). The Vancouver island seismic project: a co-crust onshore-offshore study of a convergent margin. Can. J. Earth Sci. **20**, pp. 719-741.

Finn, L., T. Onur, and C. E. Ventura (2004). Microzonation: Development and Applications. Recent Advances in Earthquake Geotechnical Engineering and Microzonation, 3-26; Kluwer Academic Publishers.

Flük, P., Hyndman, R. D., and K. Wang (1997). 3-D dislocation model for great earthquakes of the Cascadia subduction zone. J. Geophys. Res. 102, 20,539-20,550.

Frankel, A., Mueller, C., Barnard, T., Perkins, D., Leyendecker, E., Dickman, N., Hanson, S., and M. Hopper (1996). National seismic-hazard maps: documentation June 1996. U. S. Geol. Surv. Open-File Report 96-532, 110 pp.

Frankel, A., D. Carver, E. Cranswick, M. Meremonte, T. Bice, and D. Overturf (1999). Site response for Seattle and source parameters of earthquakes in the Puget Sound region. Bull. Seism. Soc. Am. **89,** 468–483.

Frankel, A., D. Carver, and R. A. Williams (2002). Nonlinear and linear site response and basin effects in Seattle for the M 6.8 Nisqually, Washington, earthquake. Bull. Seism. Soc. Am. **92,** 2090–2109.

Furumura, T., and S. K. Singh (2002). Regional wave propagation from Mexican subduction zone earthquakes: the attenuation functions for interplate and inslab events. Bull. Seism. Soc. Am., **92**, 2110-2125.

Graindorge, D., G. Spence, P. Charvis, J. Y. Collot, R. Hyndman, and A. M. Tréhu (2003). Crustal structure beneath the strait of Juan de Fuca and southern Vancouver island from seismic and gravity analysis. J. Geophys. Res., **108**, B10, 2484.

Gregor, N. J., Silva, W. J., Wong, I. G., and R. Youngs (2002). Ground-motion attenuation relationships for Cascadia subduction zone megathrust earthquakes based on a stochastic finite-fault modeling. Bull. Seism. Soc. Am., **92**, 1923-1932.

Hanks, T., and R. McGuire (1981). The character of high-frequency strong ground motion. Bull. Seism. Soc. Am., **71**, 2071-2095.

Hunter, J. (1995). Shear wave velocities of Holocene sediments, Fraser river delta, British Columbia. Current Research 1995-A, Geological Survey of Canada, 29–32.

Hunter, J., J. Harris, and J. Britton (1997). Compressional and shear wave interval velocity data for Quaternary sediments in the Fraser River delta from multichannel seismic reflection surveys, Geological Survey of Canada Open-File Report 97-3325.

Hunter, J. A., B. Benjumea, J. B. Harris, R. D. Miller, S. E. Pullan, R. A. Burns, and R. L. Good (2002). Surface and downhole shear wave seismic methods for thick soil site investigations. Soil Dynamics and Earthquake Engineering, **22**, 931-941.

Hyndman, R. D., and K. Wang (1995). The rupture zone of Cascadia great earthquakes from current deformation data and thermal regime. J. Geophys. Res. 100, 22,133-22,154.

Ito, Y., H. Matsubayashi, H. Kimua, and T. Matsumoto (2004). Spatial distribution for moment tensor solutions of the 2003 Tokachi-oki earthquake ($M_{JMA} = 8.0$) and aftershocks. Earth Planets Space, 56, 301-306.

Iwasaki, T., H. Shiobara, A. Nishizawa, T. Kanazawa, K. Suyehiro, N. Hirata, T. Urabe, and H. Shimamura (1989). A detailed subduction structure in the Kurile trench deduced from ocean bottom seismographic refraction studies. Tectonophysics, **165**, 315-336.

Jones, M. A. (1999). Geologic framework for the Puget Sound aquifer system, Washington and British Columbia: U. S. Geological Survey, Professional Paper 1424-C, scale 1: 100000.

Joyner, W. B., R. E. Warrick, and T. E. Fumal (1981). The effect of quaternary alluvium on strong ground motion in the Coyote Lake, California, earthquake of 1979. Bull. Seism. Soc. Am., **71**, 1333-1349.

Kanamori, H., and D. L. Anderson (1975). Theoretical basis of some empirical relations in seismology. Bull. Seism. Soc. Am., **65**, 1073-1095.

Kinoshita, S. (1998). Kyoshin net (K-net). Seism. Res. Lett., **69**, 309-334.

Luco, N. and Bazzurro, P. (2007), Does amplitude scaling of ground motion records result in biased nonlinear structural drift responses?, Earthquake Engineering and Structural Dynamics, The Journal of the International Association for Earthquake Engineering and of the International Association for Structural Control, **36**, 1813-1835.

Macias, M. (2008). Ground motion attenuation, source and site effects for the September 26, 2003, M 8.1 Tokachi-Oki earthquake sequence, and implications for ground motions for great Cascadia earthquakes. Ph.D. Thesis Dissertation, Carleton University, Ottawa, Canada.

Macias, M., G. Atkinson, and D. Motazedian (2008). Ground motion attenuation, source and site effects for the September 26, 2003, M 8.1 Tokachi-Oki earthquake sequence. Bull. Seism. Soc. Am., **98**, in press.

McGuire, R., W. Silva and C. Costantino (2001). Technical basis for revision of regulatory guidance on design ground motions: Hazard and risk-consistent ground motion spectra guidelines. U.S. Nuclear Reg. Comm., Rpt. NUREG/CR-6728.

McMechan, G. A., and G. Spence (1983). P-wave velocity structure of the Earth's crust beneath Vancouver island. Can. J. Earth Sci. **20**, pp. 742-752.

Mendoza, C., S. Hartzell, and T. Monfret (1994). Wide-band analysis of the 3 March 1985 central Chile earthquake: overall source process and rupture history. Bull. Seism. Soc. Am., **84**, 269-283.

Motazedian, D., and G. Atkinson (2005). Stochastic finite-fault modeling based on a dynamic corner frequency. Bull. Seism. Soc. Am., **95**, 995-1010.

Niazi, M., and K. Chun (1989). Crustal structure in the southern Bering shelf and the Alaska peninsula from inversion of surface-wave dispersion data. Bull. Seism. Soc. Am., **79**, 1883-1893.

Nishizawa, A. and K. Suyehiro (1986). Crustal structure across the Kurile trench off south-eastern Hokkaido by airgun-OBS profiling. Geophys. J. R. Astr. Soc, **86**, 317-397.

Ordaz, M., and S. K. Singh (1992). Source spectra and spectral attenuation of seismic waves from Mexican earthquakes, and evidence of amplification in the hill zone of Mexico City. Bull. Seism. Soc. Am., **82**, 24-43.

Ramachandran, K., R. D. Hyndman, and T. M. Brocher (2005). Regional P-wave velocity structure of the northern Cascadia subduction zone. J. Geophys. Res. ??.

Satake, K., K. Shimazaki, Y. Tsuji, and K. Ueda (1996). Time and size of a giant earthquake in Cascadia inferred from Japanese tsunami records of January 1700. Nature **179**, 246-249.

Siddiqqi, J. and G. Atkinson (2002). Ground motion amplification at rock sites across Canada, as determined from the horizontal-to-vertical component ratio. Bull. Seism. Soc. Am., **92**, 877-884.

Singh, S. K., Ordaz, M., Anderson, J., Rodríguez, M., Quaas, R., Mena, E., Ottaviani, M., and D. Almore (1989). Analysis of near-source strong –motion recordings along the Mexican subduction zone. Bull. Seism. Soc. Am., **79**, 1697-1717.

Valdes, C. M., W. D. Mooney, S. K. Singh, R. P. Meyer, C. Lomnitz, J. H. Luetgert, C. E. Helsley, B. T. R. Lewis, and M. Mena (1986). Crustal structure of Oaxaca, Mexico, from seismic refraction measurements. Bull. Seism. Soc. Am., **76**, 547-563.

Wells, D. L., and K. J. Coppersmith (1994). New empirical relationships among magnitude, rupture length, rupture width, rupture area, and surface displacement. Bull. Seism. Soc. Am., **84**, 974-1002.

Williams, R. A., Stephenson, W. J., Odum, J. K., and Worley, D. M. (1999). Surface seismic reflection/refraction measurements of near surface P and S wave

velocities at earthquake recording stations, Seattle, Washington. Seismological Research Letters, v. 70, no. 2, p. 257.

Yagi, Y. (2004). Source rupture process of the 2003 Tokachi-oki earthquake determined by joint inversion of teleseismic body wave and strong ground motion data. Earth Planets Space, **56**, 311-316.

Youngs, R., S. Chiou, W. Silva, and J. Humphrey (1997). Strong ground motion attenuation relationships for subduction zone earthquakes. Seism. Res. Lett., **68**, 58-73.

Table 1 - Source, path and site parameters used in simulations of PSA for the 2003, Tokachi-Oki main shock (**M** 8.1) and some of its after shocks (**M**: 7.3, 6.4, 5.9, 5.5).

	Parameter	**M** 8.1	**M** 7.3	**M** 6.4	**M** 5.9	**M** 5.5
S o u r c e	orientation (deg) [strike, dip]	[250, 17]	[208, 18]	[244, 17]	[227, 28]	[148, 48]
	dimensions (km) [strike, dip]	[132 x 168]	[60 x 24]	[19 x 10]	[10 x 6]	[6 x 4]
	depth range (km)	[6 – 56]	[43 – 51]	[34 – 37]	[53 – 56]	[47 – 50]
	Location (top) (deg) [lat., lon.]	[145.0, 41.2]	[143.8, 41.9]	[144.7, 42.3]	[145.2, 42.1]	[144.0, 42.5]
	number of sub-sources [strike, dip]	[24, 21]	[10, 4]	[3, 2]	[2, 1]	[1, 1]
	pulsing area (%)	50	✓	✓	✓	✓
	slip distribution	Yagi (2004)	random	random	random	Random
P a t h	an-elastic attenuation $Q = Q_0 f^{\eta}$	$135\,f^{0.76}$	✓	✓	✓	✓
	geometric spreading	$1 / R$	✓	✓	✓	✓
	Distance duration term [d] (s/km)	0.09	0.07	0.07	0.07	0.07
S i t e	κ factor	0.045	✓	✓	✓	✓
	amplification factors [reference level]	NEHRP C; i =45.0° [see Table 2]	✓	✓	✓	✓
	shear wave velocity [crustal] (km/s)	3.6	✓	✓	✓	✓
	density (g/cm^3) [crustal]	2.8	✓	✓	✓	✓
	damping factor (%) [PSA]	5	✓	✓	✓	✓

Table 2 – Selected earthquakes for stress drop comparisons. Source parameters from HRV catalogue. Codes for regions are as in Atkinson and Boore (2003).

Region	M	Date	Lat. [deg]	Lon. [deg]	Depth [km]	Strike-Dip [deg]	
Alaska	6.0	1983 02 14	54.51	-158.98	39.8	256	25
(AL)	6.6	1985 10 09	54.84	-159.40	31.8	246	16
Chile	8.0	1985 03 03	-33.92	-071.71	40.7	11	26
(CC)	7.1	1985 04 09	-34.26	-071.86	46.6	0	21
Japan	7.6	1978 06 12	38.02	142.07	37.7	184	14
(JA)	7.0	1982 07 23	35.98	141.91	27.0	203	14
	7.7	1983 05 26	40.44	138.87	12.6	16	27
Japan	5.8	1996 06 02	27.27	128.57	42.0	228	29
(JK)	5.9	1997 05 11	37.09	140.91	57.9	160	47
	6.1	1997 07 14	43.19	146.47	34.0	236	28
Mexico	8.0	1985 09 19	17.91	-101.99	21.3	301	18
(ME)	7.6	1985 09 21	17.57	-101.42	20.8	296	17
	7.0	1986 04 30	18.25	-102.92	20.7	290	18
	7.4	1995 09 14	16.73	-098.54	21.8	289	15
	5.6	1996 04 23	17.13	-101.84	36.8	121	59
	6.6	1996 07 15	17.50	-101.12	22.4	297	21

Table 3 – Best estimate of stress drop values for each of the selected earthquakes; the range of stress drop values that is judged to be permitted by the data variability for each case is also included.

Region	M	$\Delta\sigma$ (bars) [average]	$\Delta\sigma$ (bars) [range]
Alaska (**AL**)	6.0	30	20 – 40
	6.6	40	30 – 50
	Region	35	20 – 50
Chile (**CC**)	8.0	100	30 – 170
	7.1	120	70 – 170
	Region	110	30 – 170
Japan (**JA**)	7.6	170 [n/a]	160 – 180
	7.9	150 [n/a]	130 – 170
Japan (**JK**)	5.7	170 (?)	170 - ?
	6.3	90	60 – 120
	5.9	170 (?)	70 - ?
	6.1	30	10 – 50
Mexico (**ME**)	8.0	90 [n/a]	60 – 120
	7.6	70	30 – 120
	7.0	40	10 – 70
	7.4	40	10 – 70
	6.6	60	40 – 80
	Region	65	10 – 120

Table 4 - Source, path and site parameters used in simulations of PSA for the 12 analyzed seismic scenarios (4 magnitudes at 3 sites) of the Cascadia subduction zone. Parameters for **M** 9.0 are related to the geometry (c) in Figure 10.

	Parameter	Location	M 7.5	M 8.0	M 8.5	M 9.0
Source	orientation (deg) [strike, dip]	FRA	[315, 10]	[315, 10]	[310, 10]	[330, 06]
		VIC	[315, 08]	[315, 08]	[315, 08]	[330, 06]
		SEA	[345, 06]	[345, 06]	[345, 06]	[345, 06]
	dimensions (km) [strike, dip]	All	[80 x 30]	[170 x 90]	[380 x 90]	[600 x 150]
	depth (km) [top of fault plane]	All	10	✓	✓	✓
	Location (top) (deg) [lat., lon.]	FRA	[-124.8,48.2]	[-125.2,47.7]	[-124.5,47.1]	[-124.2,44.9]
		VIC	[-124.6,47.9]	[-124.7,47.2]	[-124.1,46.5]	[-124.2,44.9]
		SEA	[-124.3,46.9]	[-124.7,46.4]	[-124.7,45.3]	[-124.7,44.2]
	number of sub-sources [strike, dip]	all	[8, 3]	[17, 9]	[38, 9]	[60, 15]
	pulsing area (%)	All	50	✓	✓	✓
	slip distribution & hypocentre location	All	random	random	Random	random
Path	an-elastic attenuation $Q = Q_0 f^{\eta}$	All	$180\,f^{0.45}$	✓	✓	✓
	geometric spreading		$b_1 = [-1.0\ ;\ -0.5]$, for $[R \le 40\ ;\ R > 40]$ (km)			
	duration term [d] (s/km)	All	0.10	0.10	0.10	0.10
Site	κ factor	FRA	0.03	✓	✓	✓
		VIC	0.02			
		SEA	0.02			
	area & amplification factors [reference level]	Vancouver (**FRA**)	→	**Pleistocene**		
		Victoria (**VIC**)	→	**NEHRP B/C**		
		Seattle (**SEA**)	→	**NEHRP B/C**		
	shear wave velocity (km/s)	FRA	3.8	✓	✓	✓
		VIC	3.8			
		SEA	3.6			
	density (g/cm³)	FRA	2.8	✓	✓	✓
		VIC	2.8			
		SEA	2.7			
	damping factor (%) [PSA]	All	5	✓	✓	✓

Table 5 – Regression coefficients for model defined by equation 4 and 5.

Frequency [Hz]	C_0	C_1	C_2	C_3	C_4
0.10	2.338	-0.6311	0.00000	0.5357	-0.0737
0.13	2.489	-0.6412	-0.00003	0.4760	-0.0629
0.16	2.569	-0.6048	-0.00024	0.4324	-0.0641
0.20	2.671	-0.5942	-0.00040	0.3822	-0.0417
0.25	2.814	-0.6108	-0.00046	0.3490	-0.0299
0.32	2.978	-0.6431	-0.00057	0.3258	-0.0103
0.40	3.104	-0.6585	-0.00063	0.2990	-0.0074
0.50	3.241	-0.6741	-0.00081	0.2696	-0.0064
0.63	3.393	-0.7101	-0.00089	0.2483	0.0103
0.79	3.453	-0.6885	-0.00119	0.2417	0.0125
1.00	3.621	-0.7376	-0.00128	0.2116	0.0328
1.26	3.733	-0.7473	-0.00159	0.2035	0.0292
1.58	3.859	-0.7746	-0.00179	0.2010	0.0153
2.00	3.999	-0.8211	-0.00195	0.1870	0.0271
2.50	4.167	-0.8854	-0.00211	0.1802	0.0258
3.16	4.303	-0.9322	-0.00231	0.1713	0.0270
4.00	4.472	-1.0133	-0.00234	0.1713	0.0255
5.00	4.746	-1.1691	-0.00212	0.1593	0.0432
6.30	4.930	-1.2671	-0.00204	0.1645	0.0301
8.00	5.209	-1.4404	-0.00163	0.1788	0.0151
10.00	5.490	-1.6257	-0.00115	0.1736	0.0261
12.60	5.676	-1.7633	-0.00071	0.1784	0.0245
15.85	5.823	-1.8889	-0.00022	0.1845	0.0160
20.00	5.843	-1.9391	0.00000	0.1813	0.0199
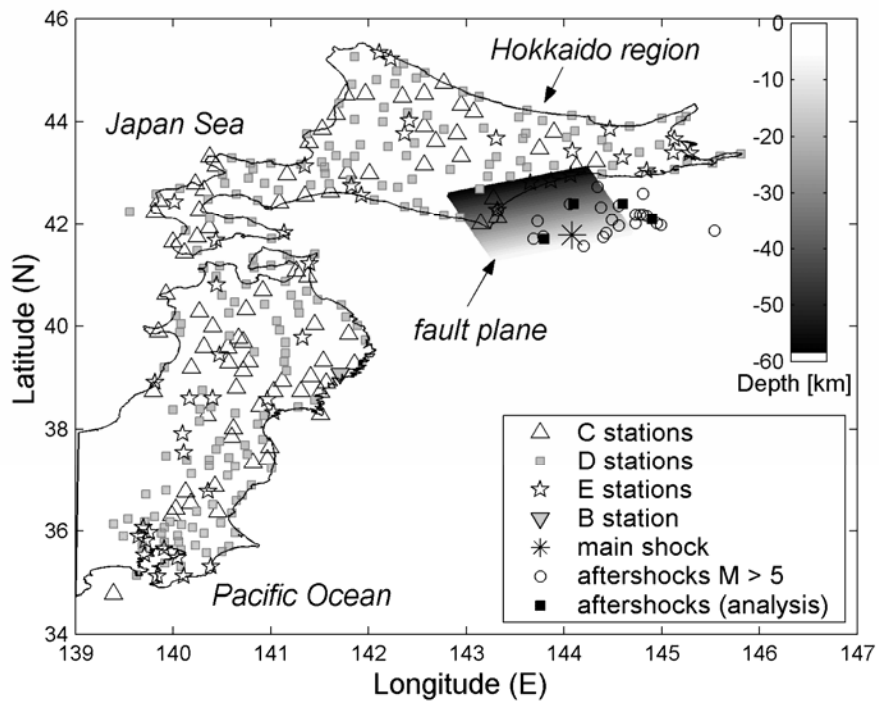
Figure 1 - K-NET, NIED seismic stations sites classified according to NEHRP (BSSC, 2001) criterion, epicenter of the September 26, 2003, **M** 8.1 Tokachi-oki earthquake (mainshock) and some of its aftershocks; black solid squares represent the analyzed aftershocks. A graphical representation of the fault plane for the main shock, modified from Yagi (2004), is also shown.
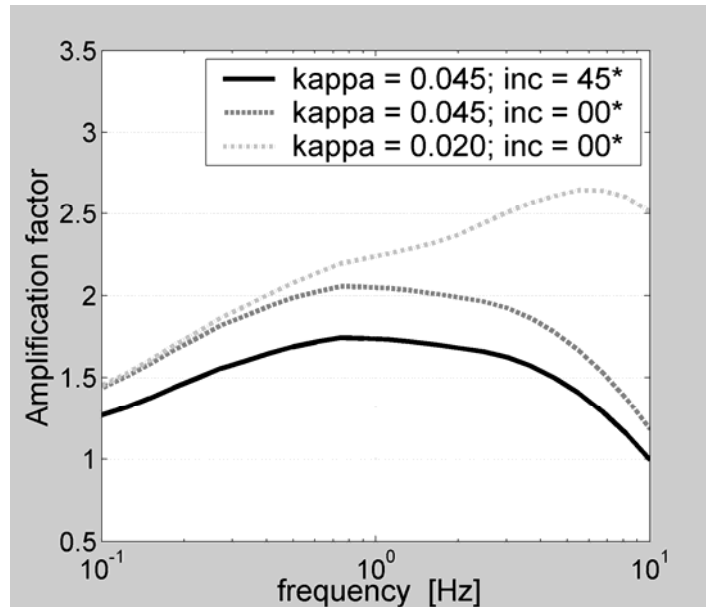
Figure 2 - Amplification functions for NEHRP C sites of the Hokkaido region, NE Japan. All these functions were calculated from a common shear wave and density profile (Table 2) but for different angles of incidence and κ factor values (as shown in the legend). Black solid line is the function reported by Macias et al. (2007), dark grey dashed line shows the effect of changing the angle of incidence and light grey dashed line shows the combined effect of changes in *i* and κ simultaneously.
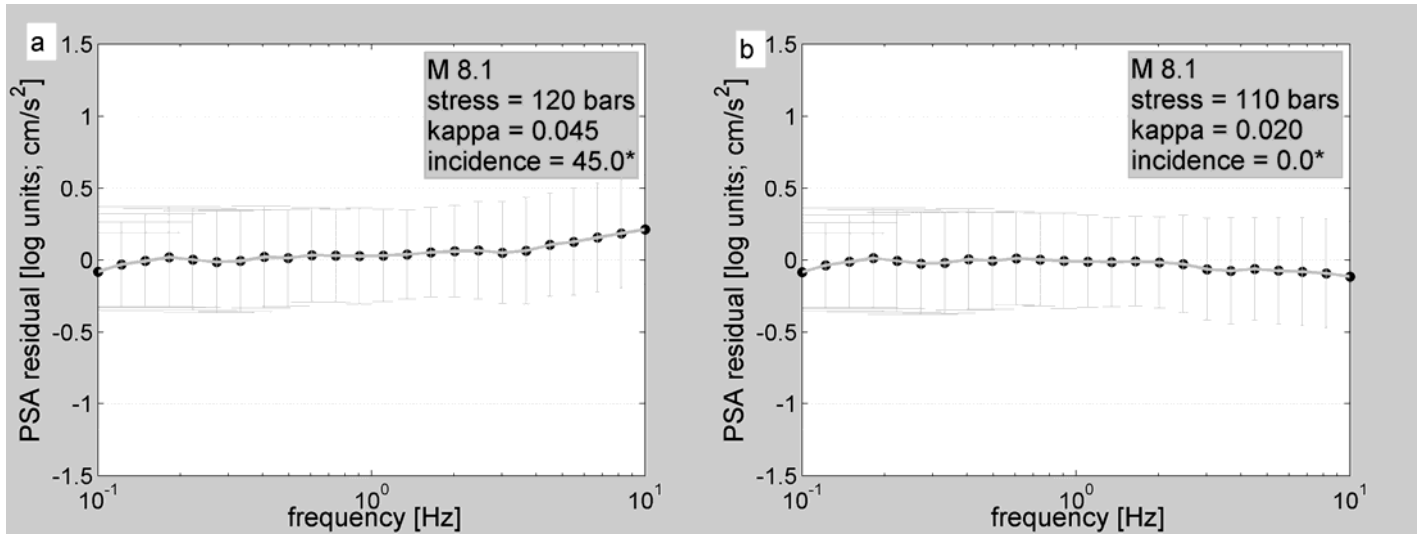
Figure 3 - Average residuals as a function of frequency, in log units, of the observed minus simulated PSA values for the **M** 8.1 Tokachi-Oki earthquake. They correspond to (a) $\Delta\sigma$ = 120 bars, i = 45.0°, κ = 0.045 and (b) $\Delta\sigma$ = 110 bars, i = 0.0°, κ = 0.02. Light grey bars are ± one standard deviation.
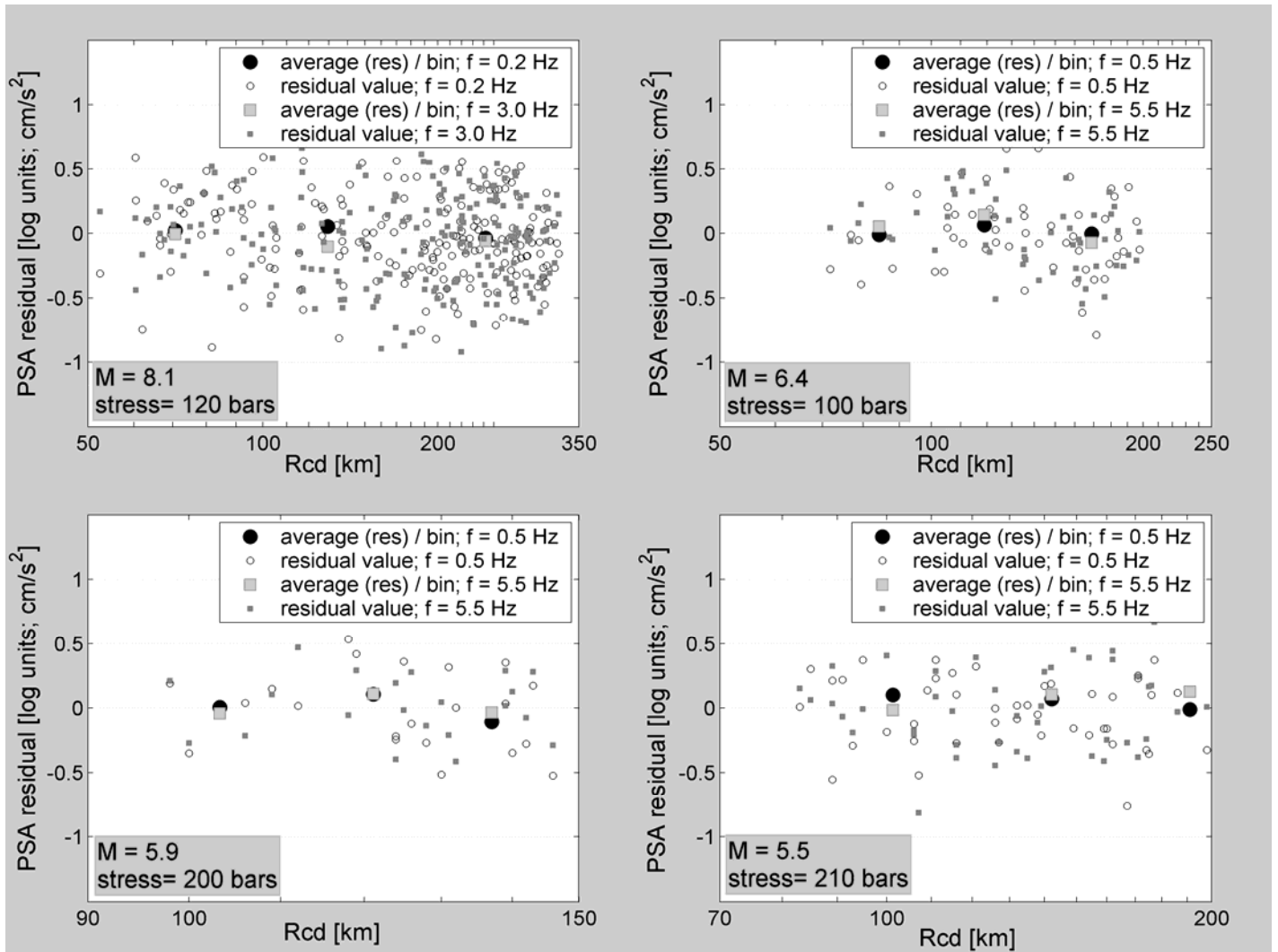
Figure 4 - Residuals of the logarithm of PSA (observed – estimated) as a function of distance (R_{cd}) for four magnitudes, at low and high frequencies. Larger symbols represent the geometric mean (log units) of the residuals contained in a specific distance bin. The distance bins were logarithmically spaced. The stress drop value that minimized residuals, for each case, is indicated in the dark grey box.
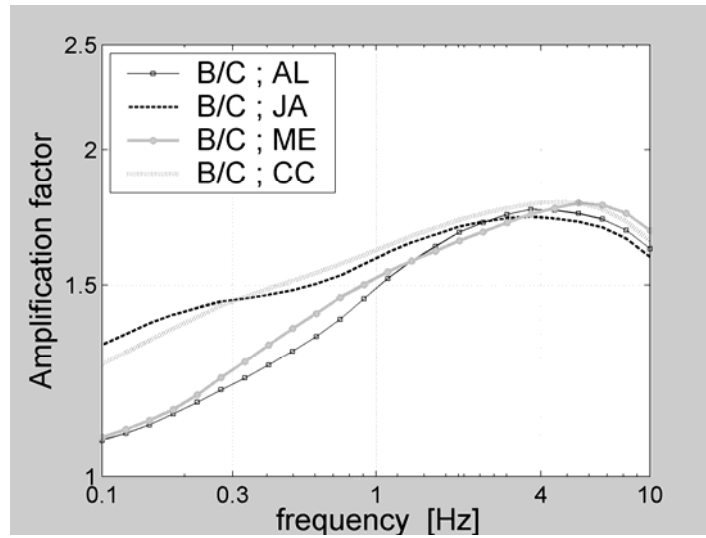
Figure 5 - Amplification functions calculated for NEHRP B/C boundary site conditions, $\kappa = 0.020$, $i = 0.0°$, for four different shear wave velocity and density crustal models, each one related to a different subduction zone (code for regions are as in Table 7).
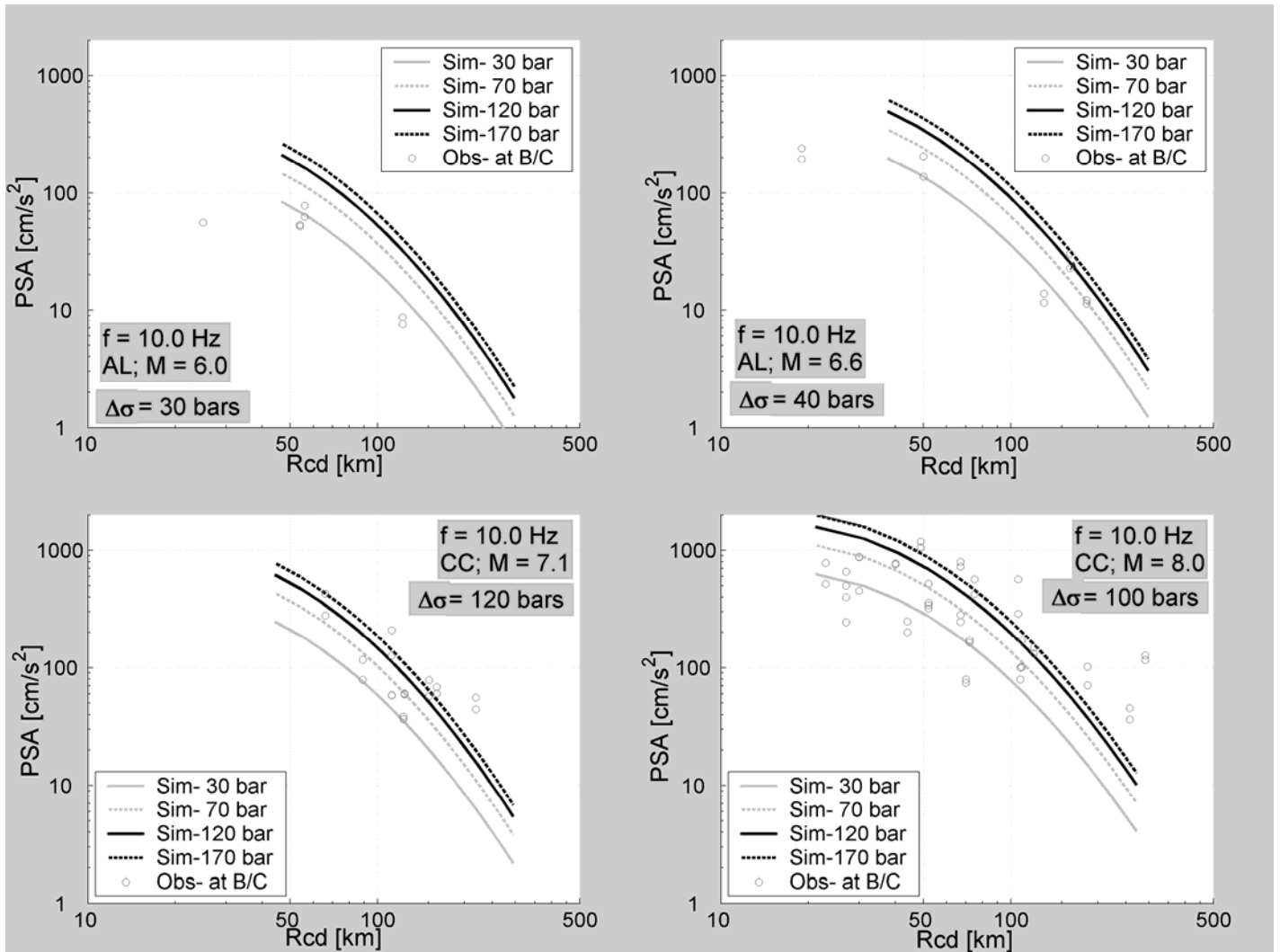
Figure 6 - PSA for interface earthquakes as a function of closest distance to fault (R_{cd}) for 10 Hz. Light gray open circles represent the data (Atkinson and Boore, 2003) corrected to NEHRP B/C boundary site condition. Lines show fits to simulated PSA ordinates for four $\Delta\sigma$ values. A separate frame is plotted for each earthquake: **M** 6.0, 6.6 in Alaska (AL) and **M** 7.1 and 8.0 in Chile (CC).
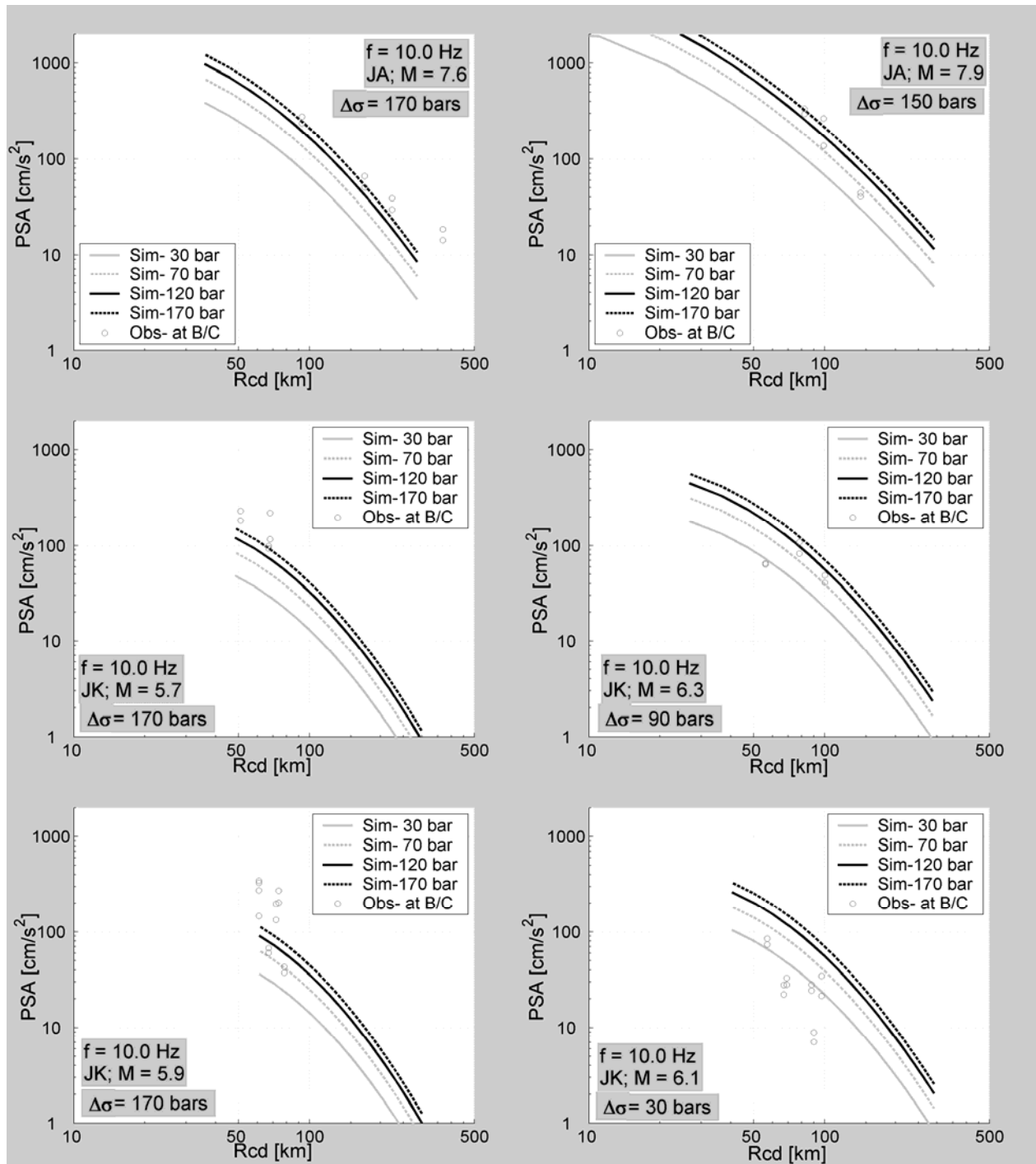
Figure 7 - PSA for interface earthquakes as a function of closest distance to fault (R_{cd}) for 10 Hz. Light gray open circles represent the data (Atkinson and Boore, 2003) corrected to NEHRP B/C boundary site condition. Lines show fits to simulated PSA ordinates for four Δσ values. A separate frame is plotted for each earthquake: **M** 7.6, 7.9, 5.7, 6.3, 5.9, and 6.1 in Japan (JA, Japanese Meteorological Agency and JK, K-NET).
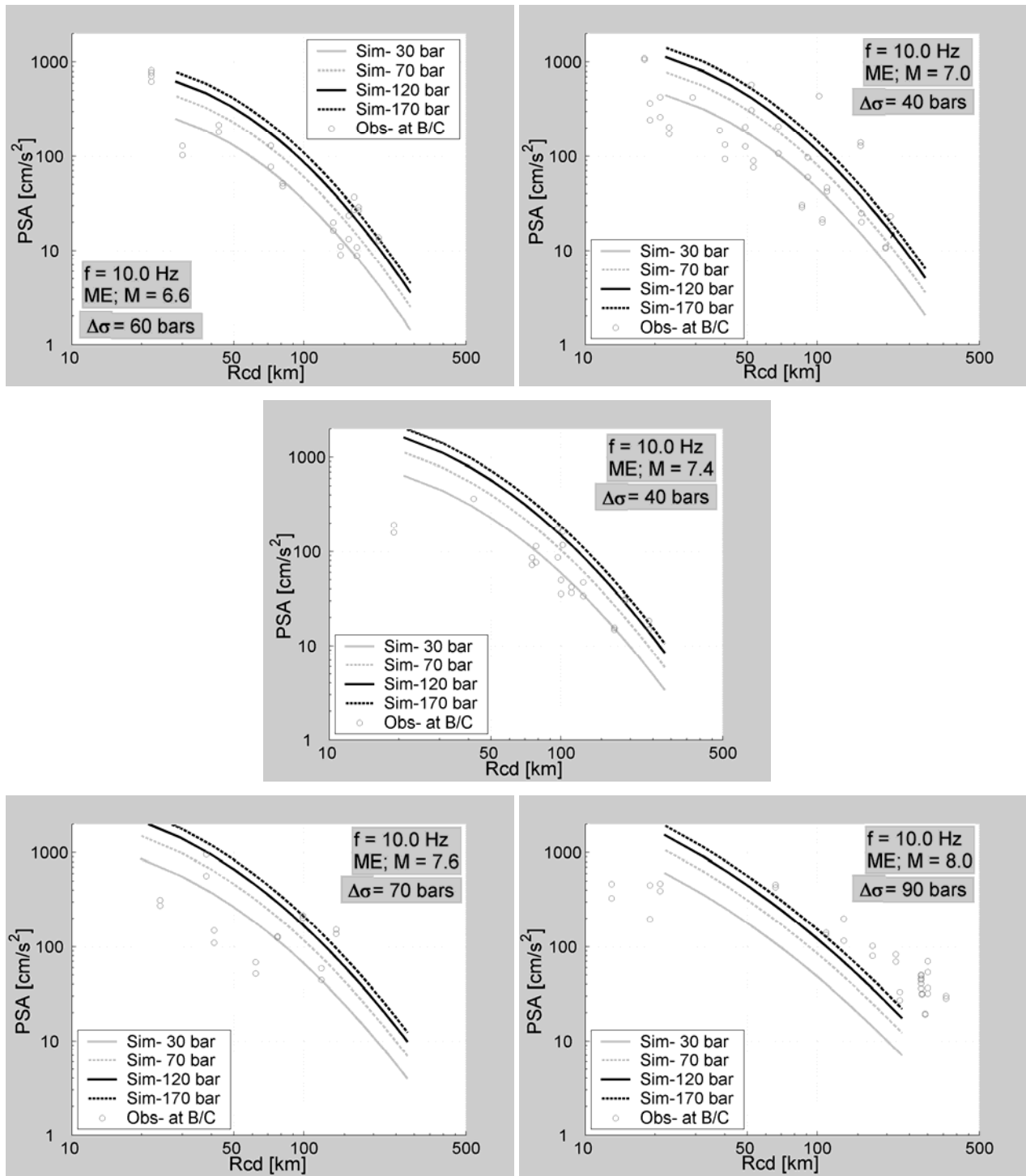
Figure 8 - PSA for interface earthquakes as a function of closest distance to fault (R_{cd}) for 10 Hz. Light gray open circles represent the data (Atkinson and Boore, 2003) corrected to NEHRP B/C boundary site condition. Lines show fits to simulated PSA ordinates for four $\Delta\sigma$ values. A separate frame is plotted for each earthquake: **M** 6.6, 7.0, 7.4, 7.6, and 8.0 in Mexico (ME).
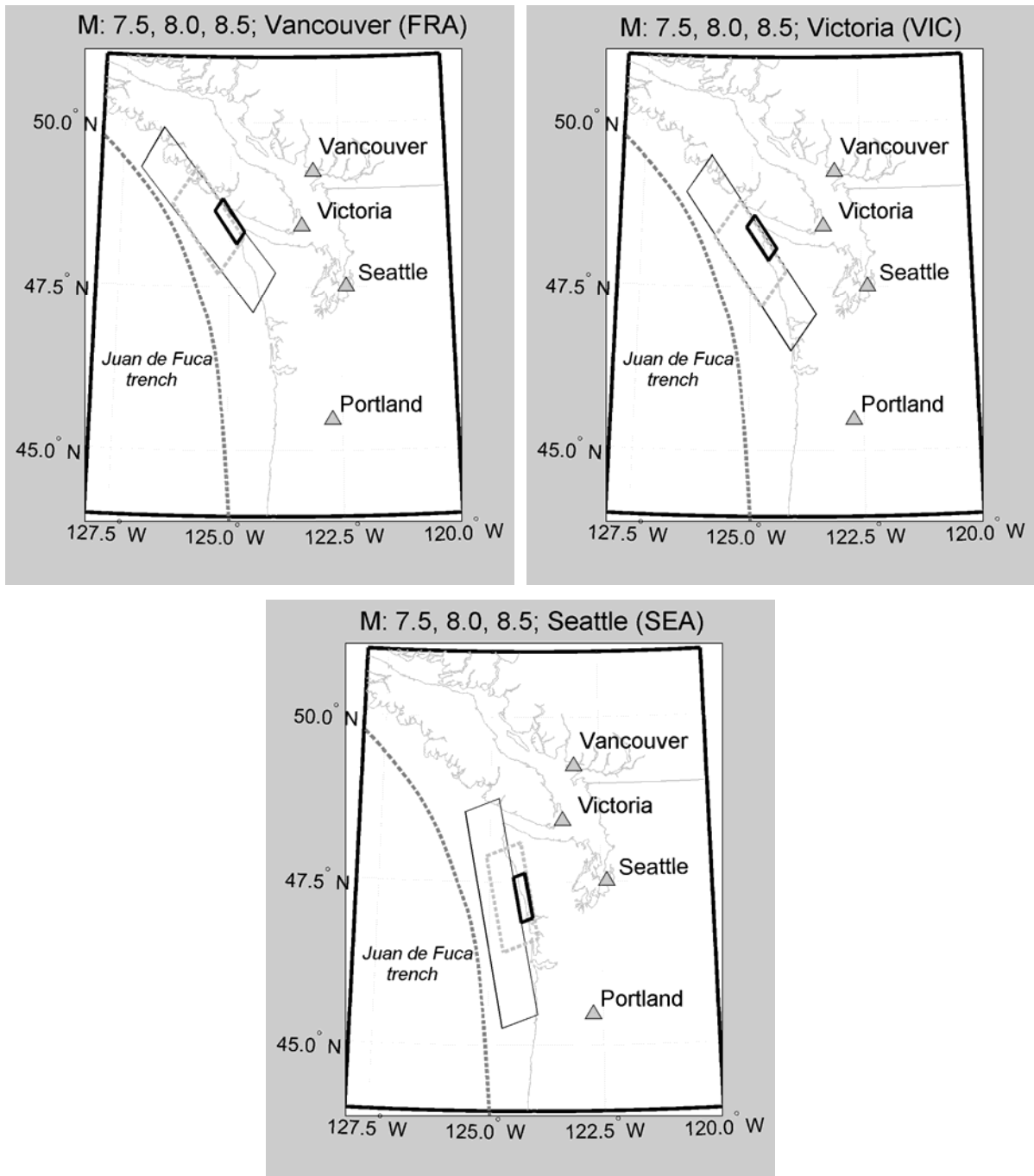
Figure 9 - Fault plane representations for scenario simulations of interface events of **M** 7.5 (black continuous line), 8.0 (light gray dotted line), and 8.5 (dark gray continuous line), as used for Vancouver (top left), Victoria (top right) and Seattle (bottom center); location, geometry, and size of fault planes given in Table 8.
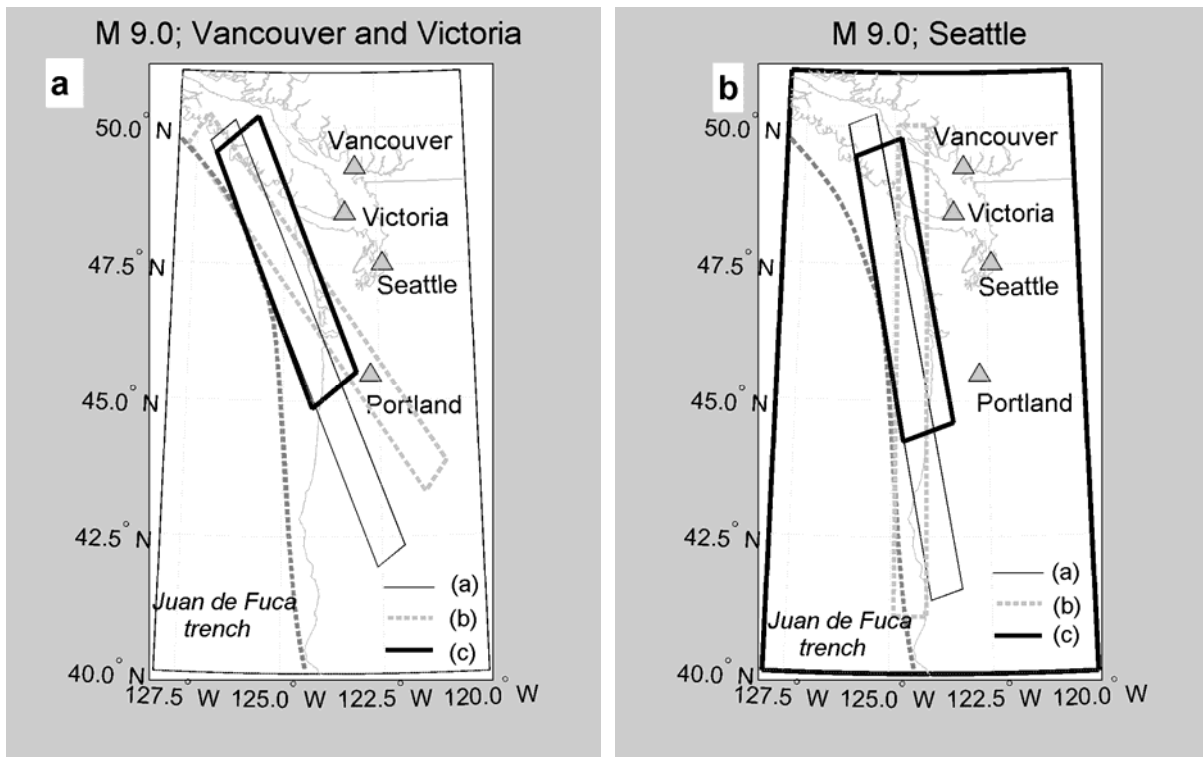
Figure 10 - Fault plane representations for scenario simulations of interface events of **M** 9 (geometries a, b and c), as used for Vancouver and Victoria (panel a), and for Seattle (panel b). Location and size of fault planes for geometries c are given in Table 8.
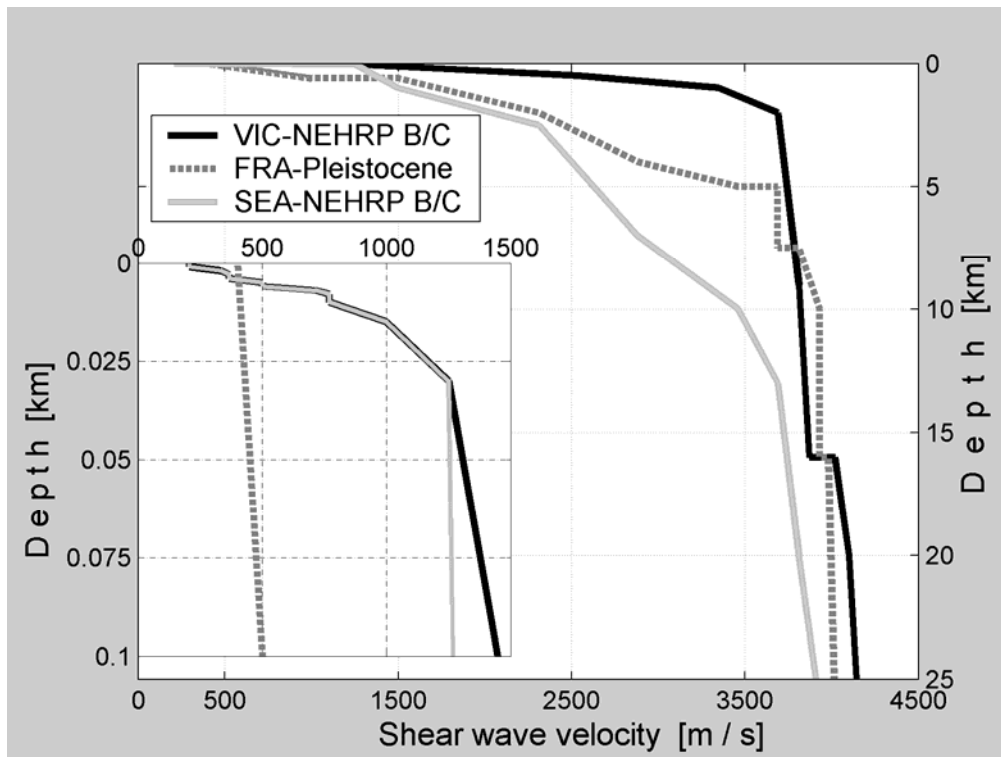
Figure 11 - Shear wave velocity models as function of depth for VIC (Victoria), FRA (Vancouver) and SEA (Seattle). Note that for FRA the reference site condition is Pleistocene (V_{S30} = 414 m/s), while for VIC and SEA it is NEHRP B/C.
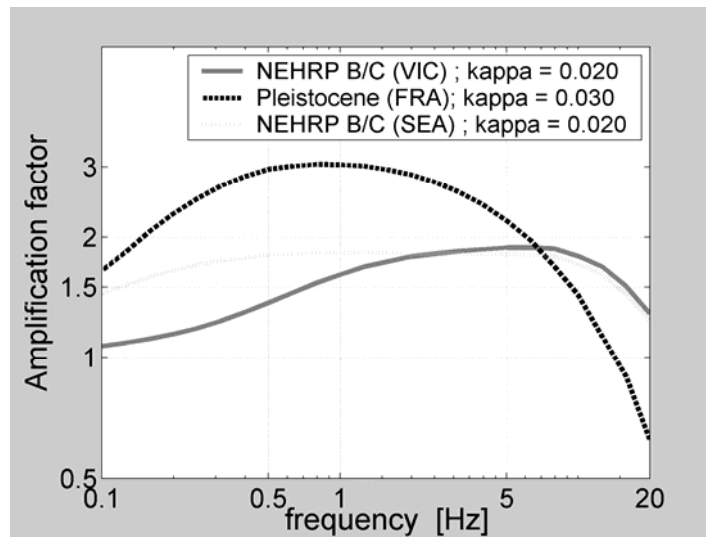
Figure 12 - Amplification factors as a function of frequency for the reference site conditions and κ values for VIC, FRA and SEA. Shear wave velocity and density models as well as the amplification factor values are given in Table 9.
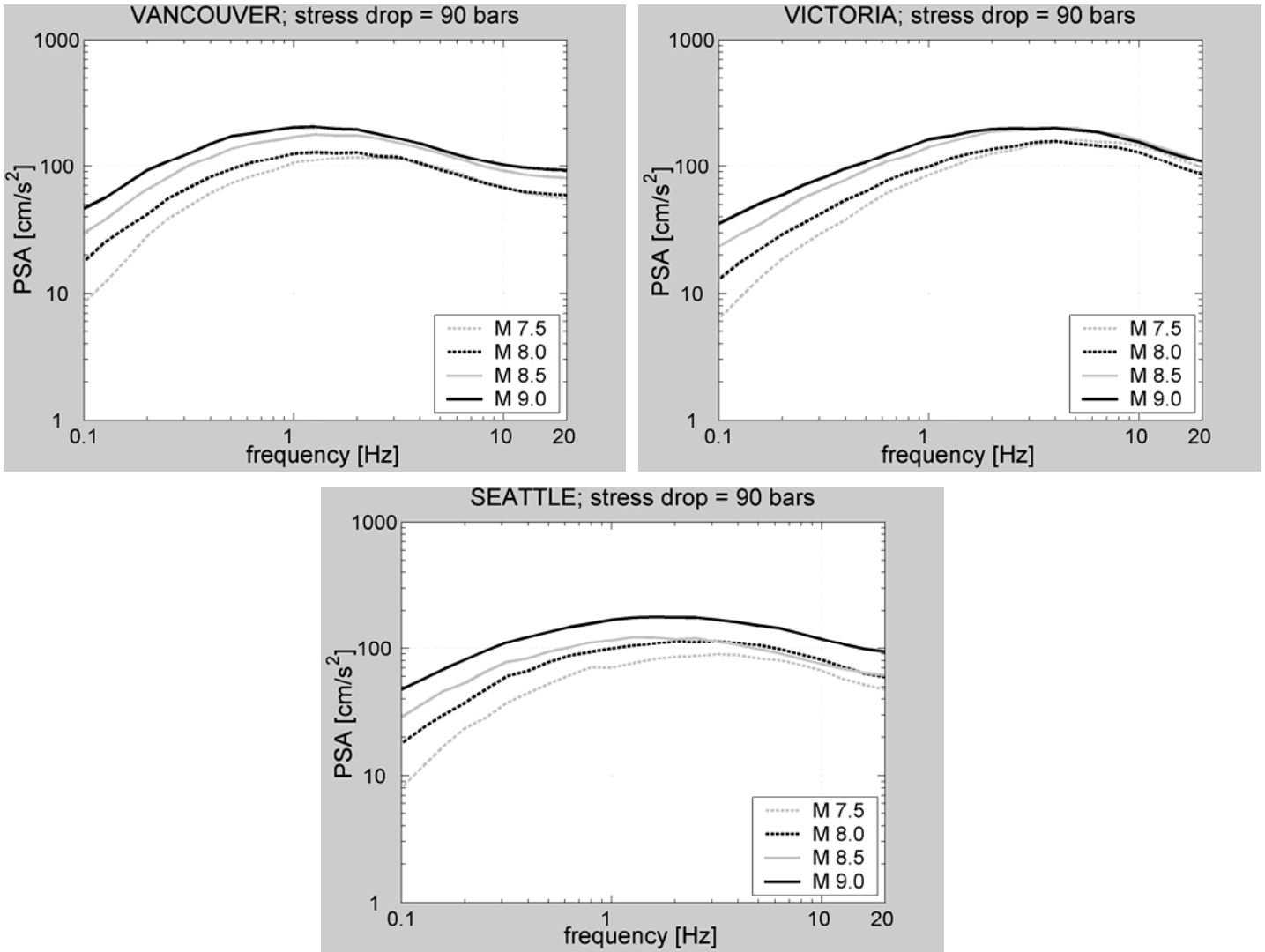
Figure 13 – Scaling of average response spectra with magnitude: **M** 7.5, 8.0, 8.5, 9.0 (c).
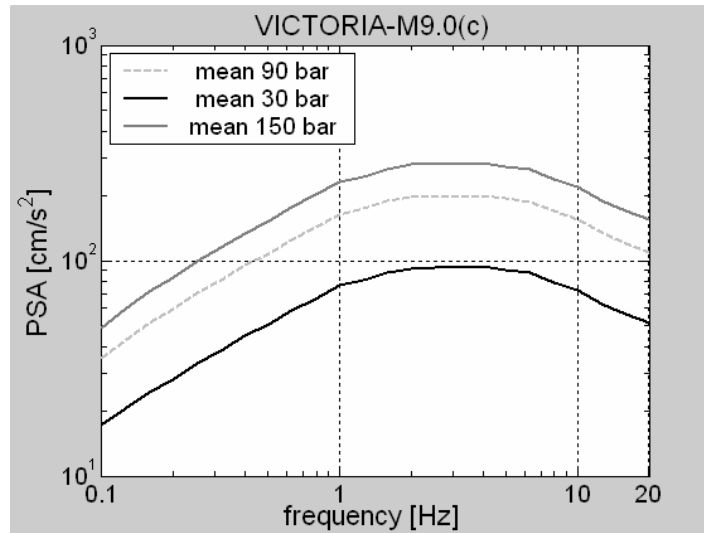
Figure 14 – Response spectra for **M** 9.0 (c) at Victoria. Light grey dashed line is the average PSA for $\Delta\sigma = 90$ bars (100 trials), light and dark solid lines are average PSA for $\Delta\sigma = 30$ and $\Delta\sigma = 150$ bars, respectively. Relative effect of stress drop at Vancouver and Seattle is very similar.
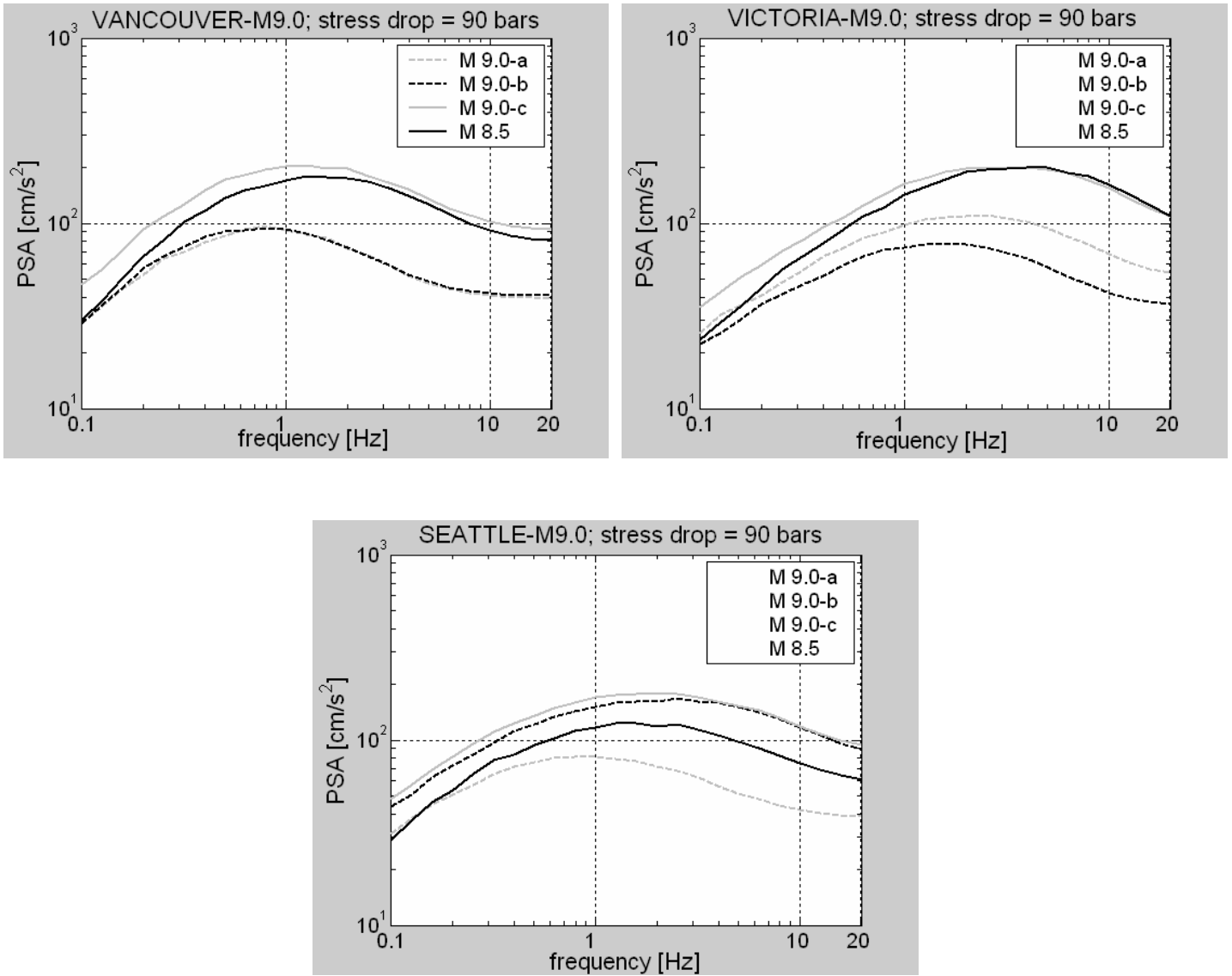
Figure 15 - Average PSA for **M** 9.0 scenarios with different geometries (a, b, and c) for Vancouver, Victoria and Seattle. Average PSA for **M**8.5 also shown for reference.
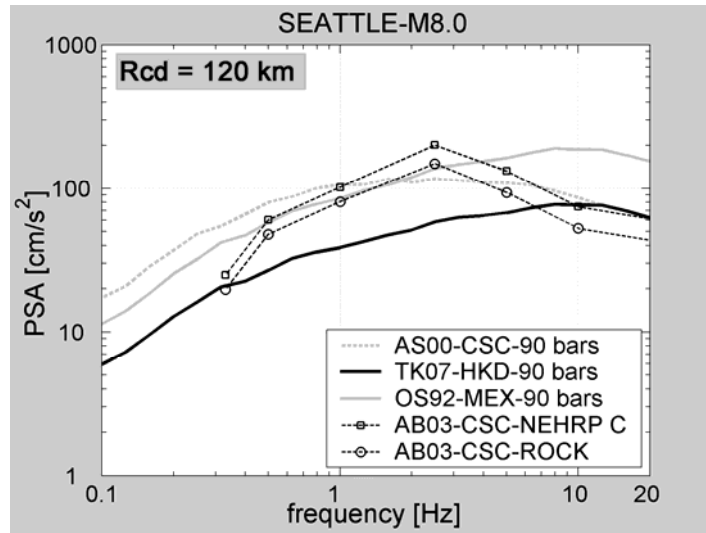
Figure 16 – Response spectra for an **M** 8.0 scenario at Seattle for different subduction zone attenuation models. AS00=Atkinson and Silva (2000), adopted for the Cascadia region; OS92 = Ordaz and Singh (1992) for the Mexican subduction zone and TK07 is the Tokachi-Oki model of Macias et al. (2007) (all for $\Delta\sigma$ = 90 bars). AB03 lines are the PSA estimates from Atkinson and Boore (2003) relationships for NEHRP C and rock site conditions at different distances and corrected by Cascadia regional factors.
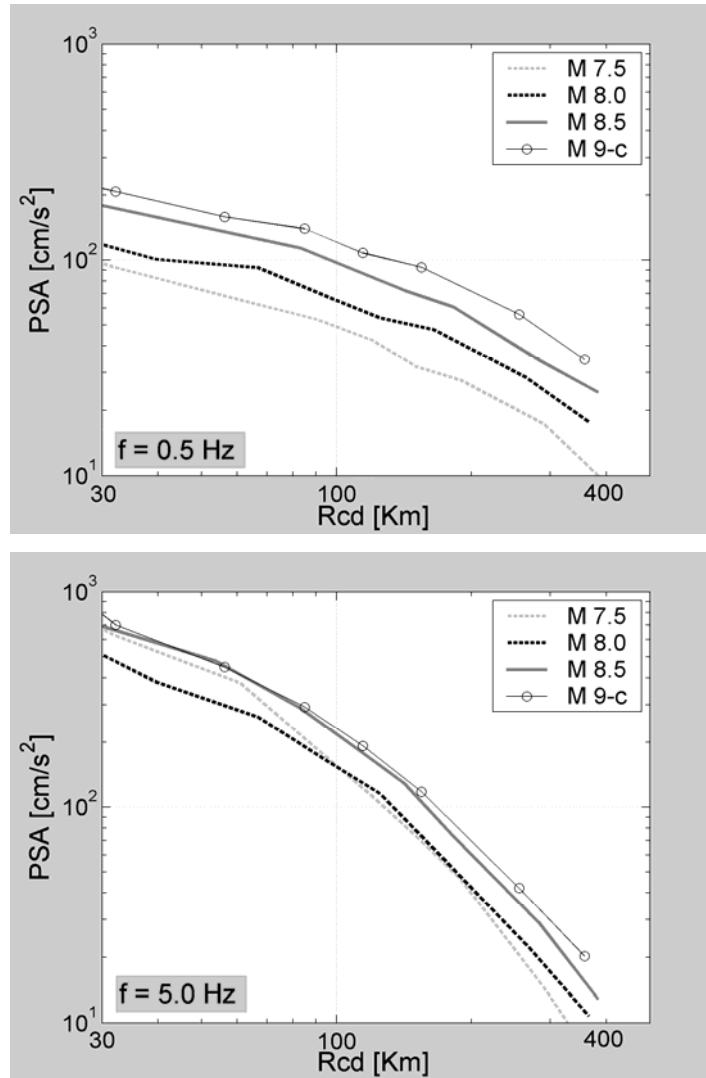
Figure 17 - Average PSA for Cascadia subduction events ("best estimate" source and path) as a function of closest distance to fault (R_{cd}) for NEHRP B/C boundary site conditions (VIC velocity model). Top panel show attenuation for **M** 7.5, 8.0, 8.5, and 9-c for 0.5 Hz, while lower panel are for 5.0 Hz. Estimates are made for perpendicular profiles from the trench.
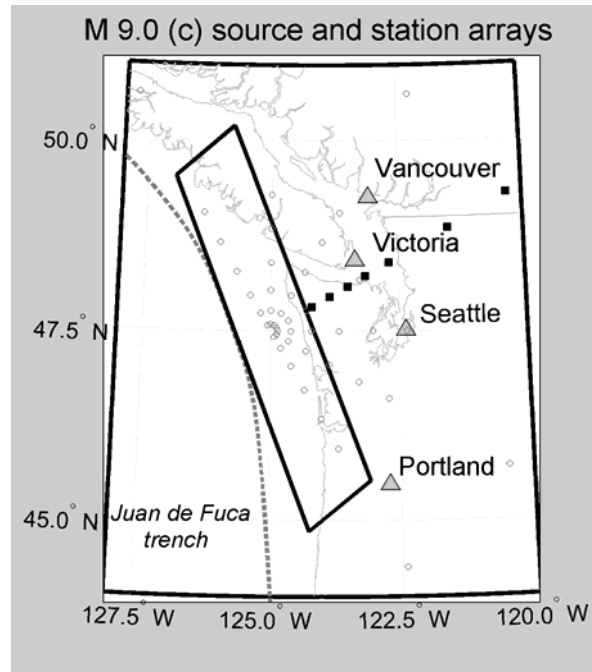
Figure 18 – Scenario seismic sources and station arrays: perpendicular profiles (black square symbols) and fan shape profiles (grey open symbols) for **M** 9.0 (c geometry).
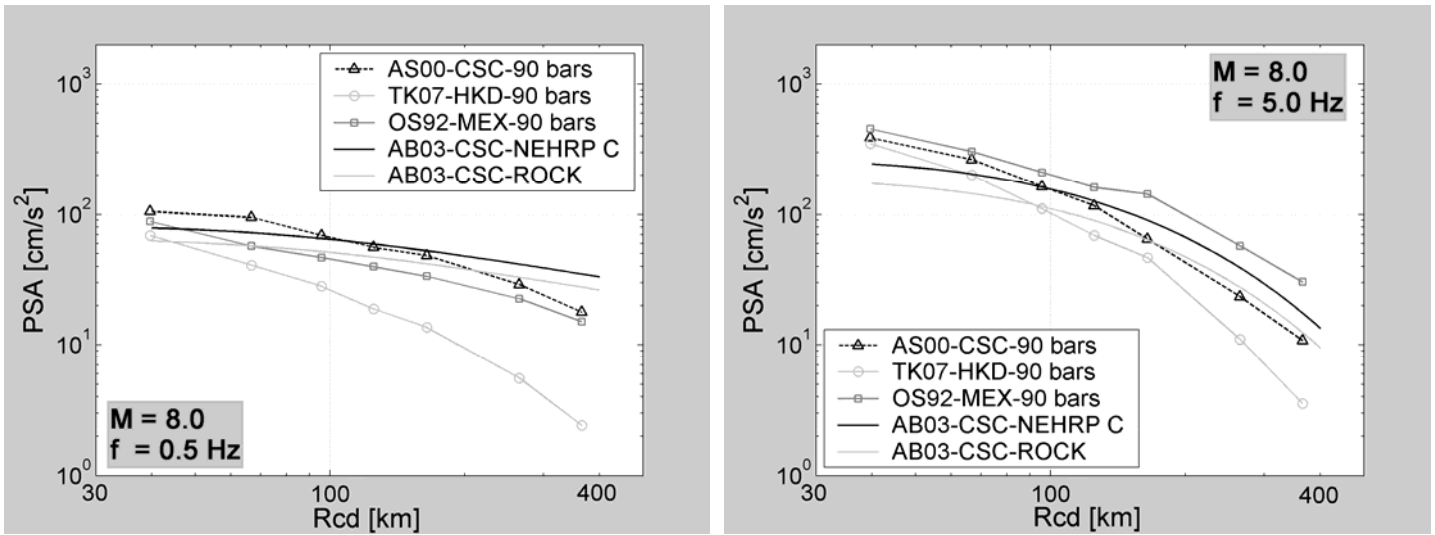
Figure 19 - Average PSA as a function of closest distance to fault (R_{cd}) (10 trials) for NEHRP B/C boundary site conditions (VIC), for a **M**8.0 event, at 0.5 and 5 Hz. Symbols depict average simulated PSA at the R_{cd} values associated with the perpendicular profile "stations" for attenuation models of Atkinson and Silva, 2000 (AS), the Tokachi-Oki model of Macias et al, 2007 (TK07), and the Mexican model of Ordaz and Singh, 1992 (OS92) (all for B/C). Lines show empirical predictions of Atkinson and Boore, 2003 (AB03) for NEHRP B (rock) and C (with the Cascadia factors).
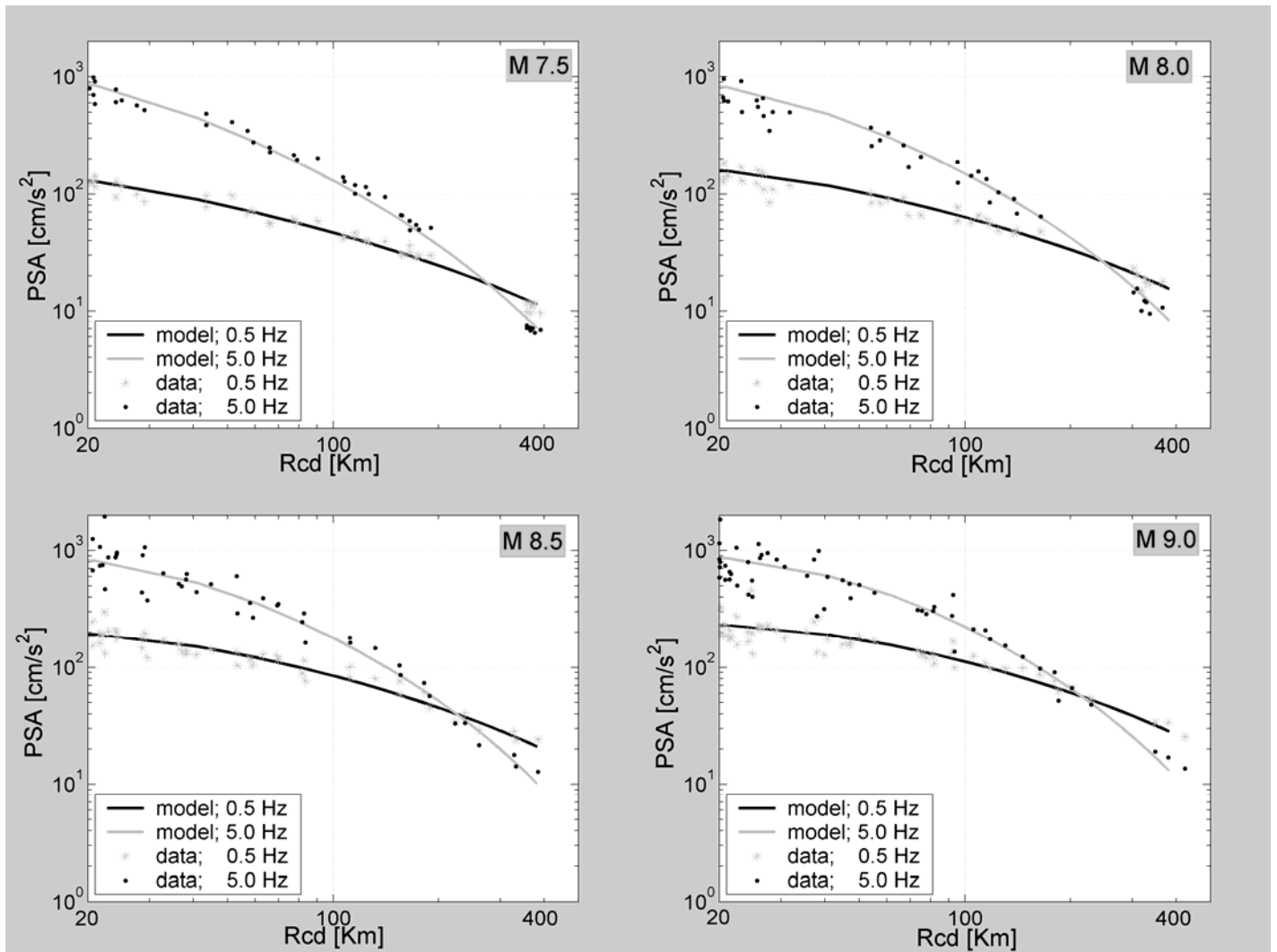
Figure 20- PSA values from simulations for a fan of sites (symbols), compared to predictions of derived ground-motion predictions equations of Table 10 (all for B/C), for **M** 7.5, 8.0, 8.5 and 9.0 (geometry c), at 0.5 and 5 Hz.
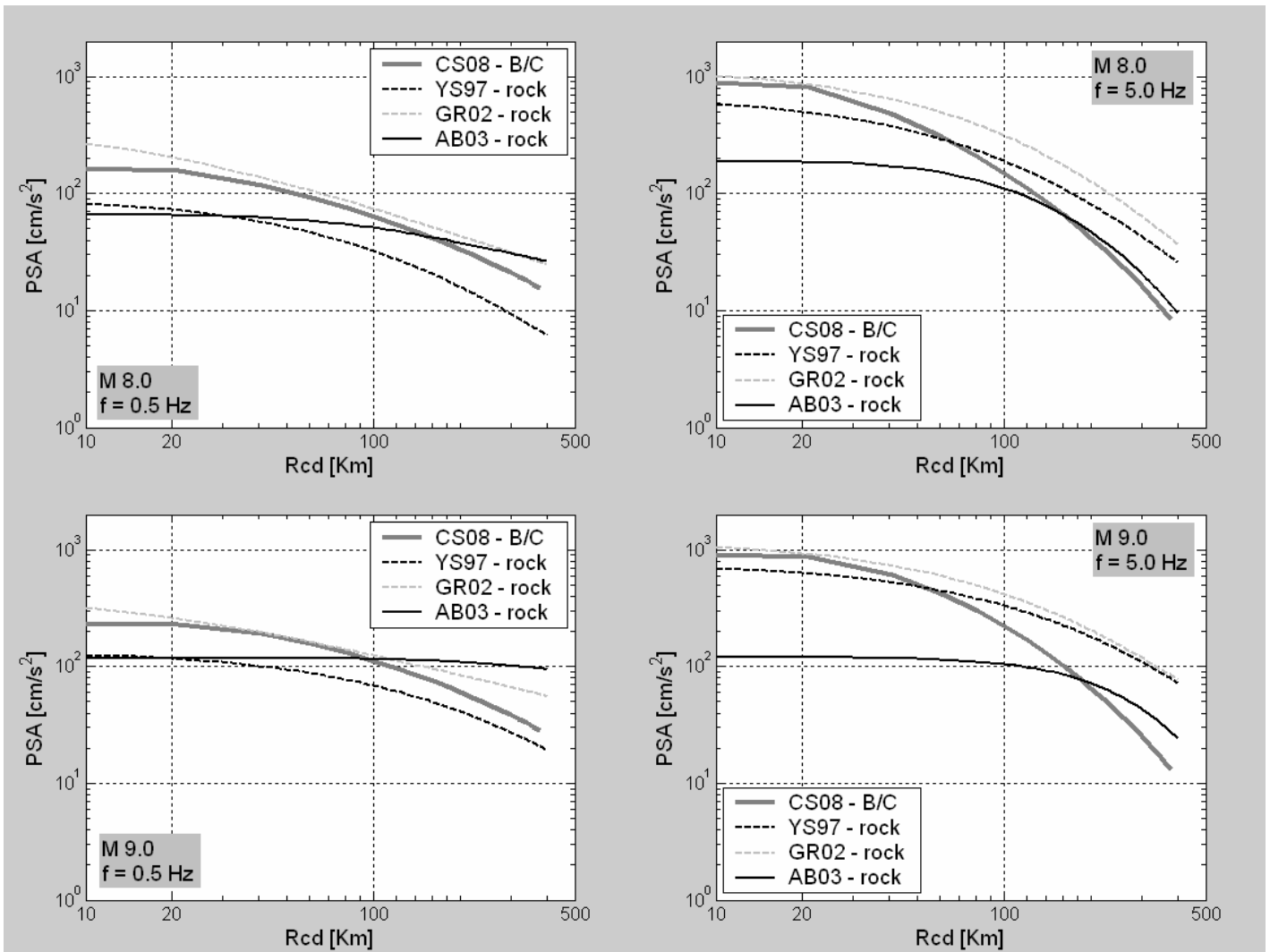
Figure 21 – Interface GMPEs of this study (CS08) for B/C conditions, compared to other study results
for rock sites, for 0.5 Hz and 5 Hz. YS97 = Youngs et al., 1997; GR02 = Gregor et al., 2002;
AB03 = Atkinson and Boore (2003) with Cascadia factors.
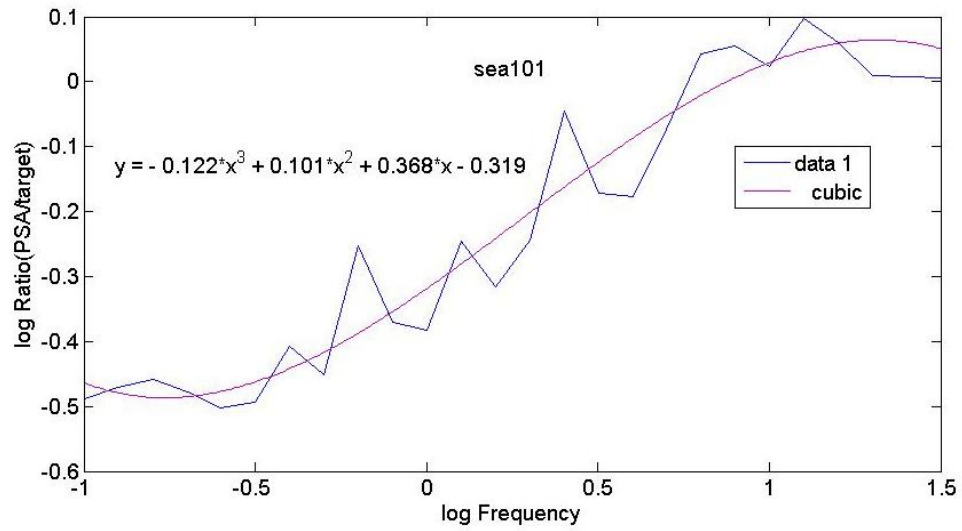
Figure 22 – Example of the ratio of the response spectrum of an input recording (Tokachi-Oki HDK084, average horizontal component) to a target spectrum (**M**8.5 at Victoria, on B/C), and the fit of overall shape by a polynomial.
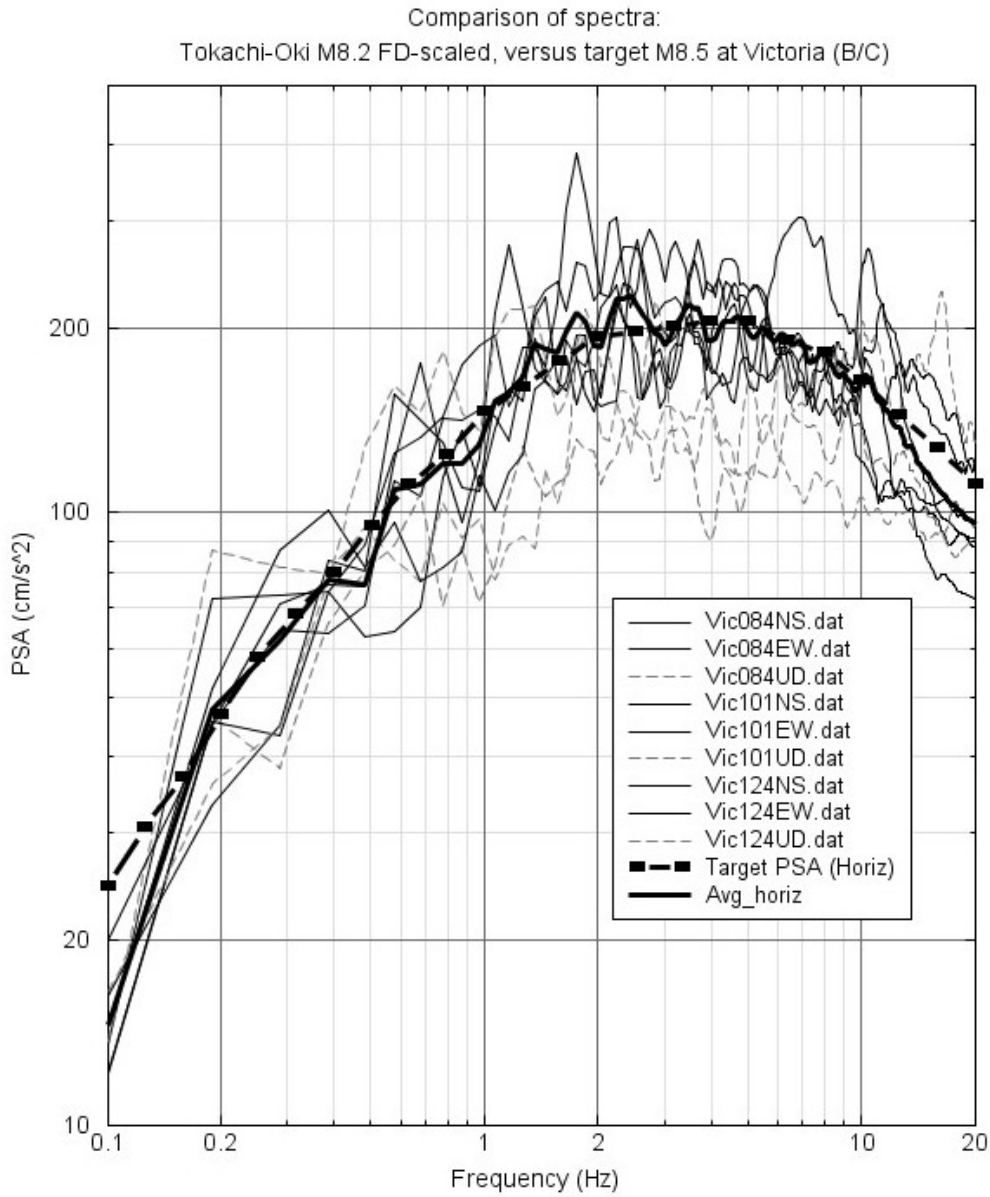
Figure 23 – Comparison of response spectra of modified time histories "matched" to the target spectrum for Victoria (B/C). Average of horizontal components (geometric mean) for the modified records is also shown.
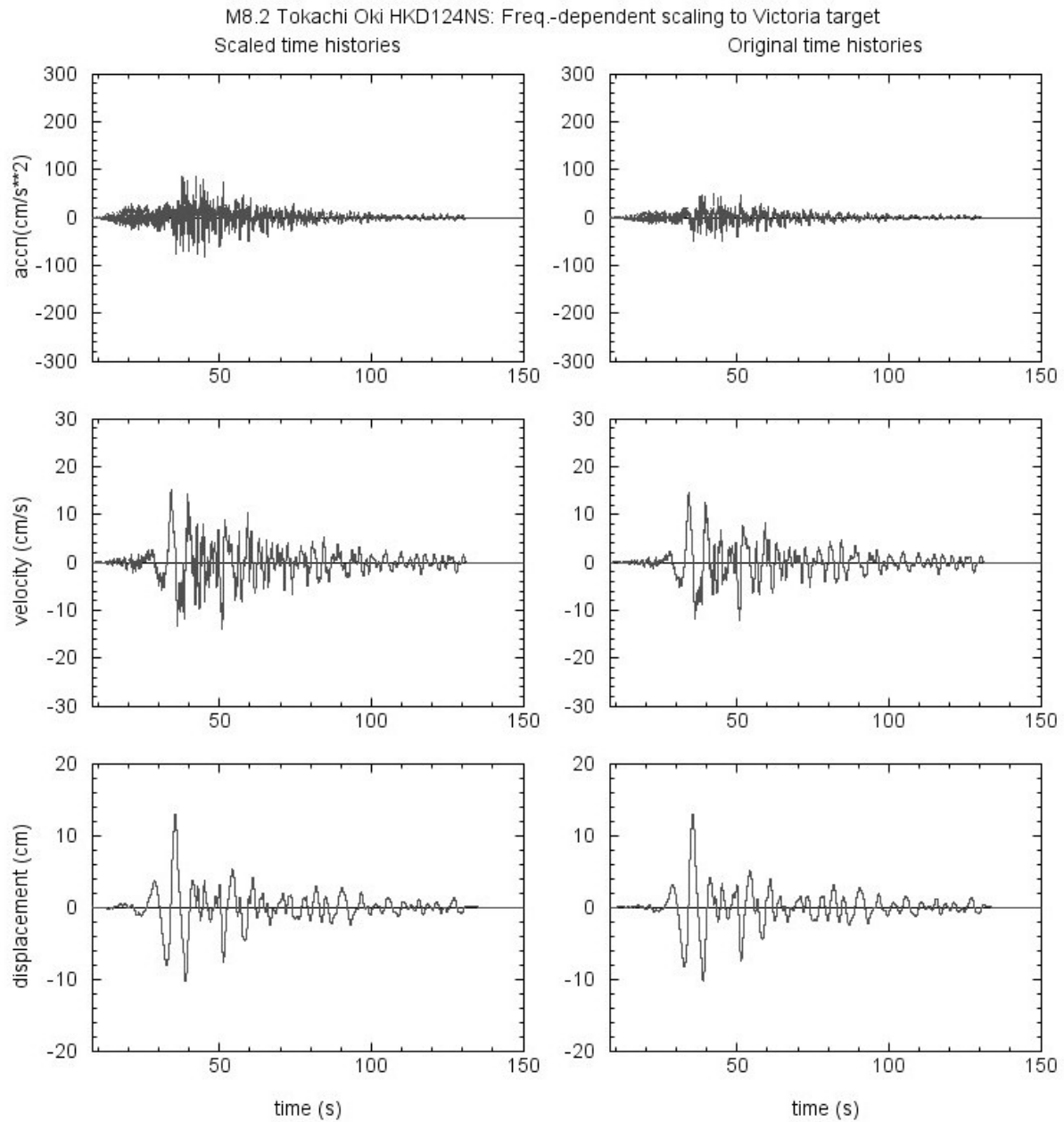
Figure 24 – Example of input and output time histories to the spectral modification method, for HDK124 (NS) matched to the Victoria target (output spectra shown on Figure 23).